Spice models for vacuum tubes using the uTracer

Derk Reefman

March 14, 2019

Contents

1 Introduction

Spice modelling of vacuum tubes has already a long history. An important prerequisite is (obviously) the availability of accurate spice models of the vacuum tubes. A second prerequisite is the availabiity of accurate data to fit the models to. In the past, many spice models have been generated based on I-V curves as published in the databooks published by the tube manufacturers. There are important limitations to this approach, most notably that it is sometimes difficult to get an accurate reading from the old graphs, the old graphs often are idealized, and, perhaps most important, the fact that only limited datasets are available for a tube. These last two short comings have been removed completely with the advent of the uTracer of Ronald Dekker[Dek13]. The uTracer is a very elegant tool, and can provide accurate representations of the tube characteristics. The variation in characteristics between tubes is substantially larger than measurement errors in the uTracer itself.

Many power tubes show substantial secondary emission effects. Those effects never received a lot of attention, because in the tube datasheets these effects where always largely ignored. After all, secondary emission was not considered something to be proud of. Still, for many designs in audio amplification, secondary emission effects can have a sizeable impact, especially for high outputs where the Ia-Va trajectory of the power tubes transverses the area where secondary emission is dominant.

Also, mixing and modulation tubes have a rich history, and spice models for these tubes are hard to find - if they exist at all. Developing a model to describe those tubes - like the ECH81 and the EF80 with g3 as modulation grid - is not possible based on the available data sheets, as those provide very little detail and only refer to what from a practical perspective was needed to design a circuit.

This and the sheer unlimited availability of tube data with the advent of the uTracer was the reason to start with the development of accurate simulation models, as much as possible based on physics of the valve, for pentodes, beam tetrodes, and hexodes/heptodes. For the pentodes, modelling secondary emission in those has received a great deal of attention. All this has resulted in a program `ExtractModel` that takes the outputfile of the uTracer, and provides a Spice simulation model as output.

2 Early Spice models for vacuum tubes

Spice models for vacuum tubes have been investigated and proposed in the early nineties already. An important milestone is the paper by Reynolds [Rey93]. Later on the work by Reynolds was complemented by Marshall [WML95] who included models for a diode, triode and pentode, all based on the fundamental Langmuir-Childs law for the diode anode current I_a:

$$I_a(V_a) = \frac{1}{k} V_a^{3/2} \tag{1}$$

This represents the famous 3/2 exponential law, which is arrived at under the assumption of a spherically symmetric space charge. This leads to a triode description below:

$$I_a(V_a, V_g) = \frac{1}{k_{G1}}(V_g + \frac{V_a}{\mu})^{3/2} \quad \text{for } V_g + V_a/\mu >= 0$$

$$I_a = 0 \quad otherwise \tag{2}$$

While for various tube types this gives a reasonable fit, and leads to good DC-operating points, the dynamic behaviour is not well-captured, especially for low anode voltages V_a. These discrepancies are caused mainly by two effects:

1. In practice, tube geometries do not exhibit cylindrical symmetry. The cathode is often more or less rectangular, the grids exhibit an elleptical geometry. Often, also the anode is far from cylindrically symmetric;

2. The grid(s) are not uniform, but rather consist of a helix-wound wire. This leads to inhomogeneous electric field distributions. A particularly well known consequence of this is the 'island effect' [Dek43], causing $I_a - V_g$ curves to display a 'remote cut-off' behaviour.

A first attempt to start including some non-ideal effects was included in the models presented in [Exc95]. It appears as if there were no fundamental physical principles that underlie the models in [Exc95]; as the models contain a large number of variables however, the models clearly provided a better fit to the observed currents than any of the models of Marshall or Reynolds. The first tube model incorporating deviations from this ideal behaviour based on some physical insight was a diode model including a contact potential ϵ and an exponent x that could deviate from 3/2 due to (non-homogeneous) space charge effects ([Per98]):

$$I_a(V_a) = \frac{1}{k}(V_a + \epsilon)^x \tag{3}$$

Especially the variable exponent proved to be very useful, as many diodes had constructions that create non-homogeneous emissions. This approach was successfully extended to other tube types by Koren, to be elaborated in the next section.

3 Korens models

Norman Koren [Kor96, Kor01] has proposed a triode and a pentode model, both models based on the variable exponent x and a number of other, new elements. In the following sections, an intermediate variable E_1 is introduced. While this variable $E_1(V_a, V_{g2}, V_{g1})$ has an explicit dependence on V_a, V_{g2} and V_{g1}, this explicit dependence will not be referenced in order to avoid cumbersome notation. As the new models that will be introduced in Sec. 4 will build on Koren's models, the next sections will present a short review of his work.

3.1 Koren Triode model

For the Koren triode model, the variable $E_1(V_a, V_{g2}, V_{g1}) \equiv E_{1,T}$ is given by:

$$E_{1,T} = \frac{V_a}{k_p} \log\left(1 + e^{k_p(1/\mu + V_g/\sqrt{k_{VB} + V_a^2})}\right) \tag{4}$$

$$I_{a,Koren}(V_a, V_g) = \frac{E_{1,T}^x}{2k_{G1}}(1 + sgn(E_{1,T})) \tag{5}$$

The function $\frac{1}{2}(1 + sgn(E_{1,T}))$ is used to guarantee that the anode current is zero for negative anode voltages. This function is not referenced further in this document, however, will be in all Spice model codes - see also Sec. 13.3. These equations describe the 'island' effect (the extra curvature at low anode current and high negative grid voltage, similar to 'remote cut-off' behaviour - see [Dek43]) in a phenomenological way. The quality of the fit is in general excellent as shown below for a regular triode PC86 as well as a ECC81, which has a much more pronounced island effect.
The quality of the fit is representative for the about 30 triodes fitted so far.

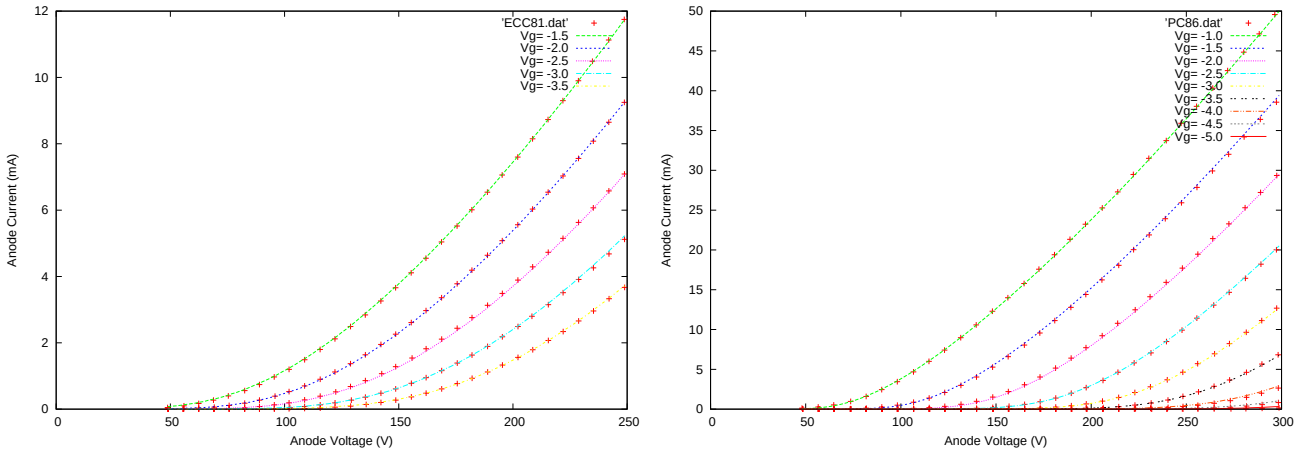

Figure 1: Koren model fits of two very different triodes, the ECC81 and PC86.

3.2 Koren pentode model

Koren made the fundamental assumption that the suppressor grid g_3 always is at zero potential. This removes the need to separately model this grid, and also is the basis for the assumption that secondary emission effects can be neglected. The function introduced by Koren for the anode current equation for pentodes is

$$E_{1,pentode} = \frac{V_{g2}}{k_p} \log\left(1 + e^{(k_p(\frac{1}{\mu} + \frac{V_g}{V_{g2}}))}\right) \tag{6}$$

$$I_a(V_a, V_{g2}, V_g) = \frac{E^x_{1,pentode}}{2k_{G1}}(1 + \mathrm{sgn}(E_{1,pentode}))\arctan\left(\frac{V_a}{k_{VB}}\right) \tag{7}$$

The pentode equation differs from the triode equation in that the screen grid replaces the plate as a controlling element, and that the k_{VB} term that is used in the triode model to mimick the 'island effect' is absent. An arctangent term (from Scott Reynolds' model) is added to model a response curve "knee" whose location is proportional to k_{VB}. Note that Koren uses the same variable name k_{VB} for two very different purposes in the triode and pentode model! In Koren's model, the screen grid current equation for pentodes is independent of V_a and given by

$$I_{g2}(V_{g2}, V_g) = (V_g + \frac{V_{g2}}{\mu})^{3/2}/k_{g2} \quad \text{for } V_g + \frac{V_{g2}}{\mu} > 0, \text{ and } I_{g2} = 0 \text{ otherwise.} \tag{8}$$

The result of a least squares fit of these models to the data of a PF86 (identical to EF86 with different heater) is provided in Fig. 2 where the modelling of the anode currents is good. The screen currents are not dependent on V_a. While for an EF86, which behaves like a text-book pentode, the fit is good, for many power pentodes and beam-tetrodes the description is far from accurate. These tubes display substantial secondary emission effects that can largely impact performance, and, therefore, should be well-characterized. Before that, the Koren pentode model will be revisited first.

3.3 Koren (Malcolm-Brown) heptode model

Recently (July 13th 2015), the author became aware of the existance of the work of Malcolm-Brown [MB14]. In this work, the original Koren model has been extended to include a hexode/heptode description. The anode current is modelled as:

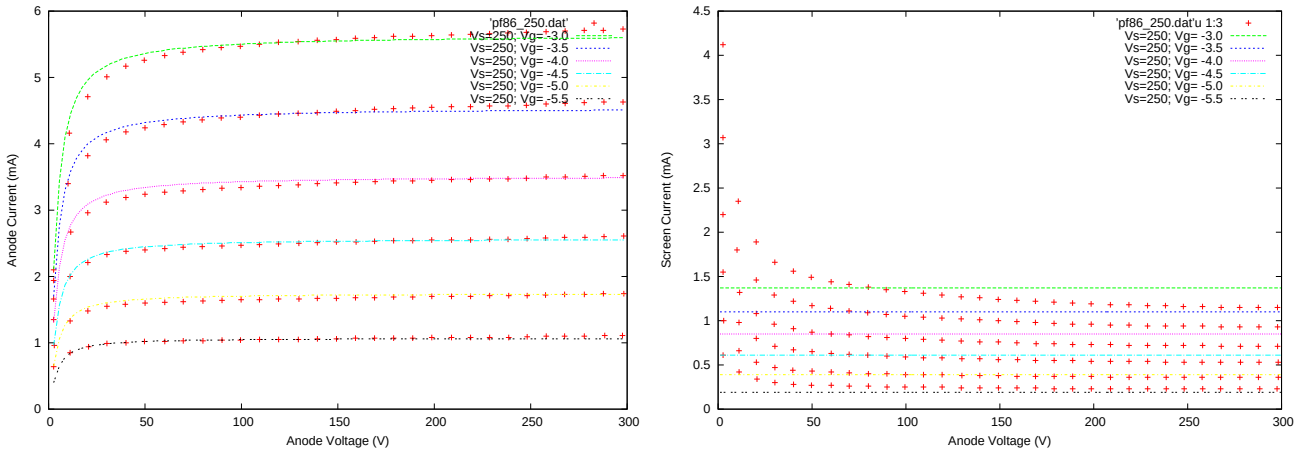

Figure 2: Koren model fits of anode and screen current of a PF86.

$$E_{1,hexode} = \frac{V_{g3}}{k_p} \log\left(1 + e^{(k_p(\frac{1}{\mu} + \frac{V_{g1}+V_{g2}}{V_{g3}}))}\right) \tag{9}$$

$$I_a(V_a, V_{g3}, V_{g2}, V_{g1}) = \frac{E^x_{1,hexode}}{2k_{G1}}(1 + \mathrm{sgn}(E_{1,hexode}))\arctan\left(\frac{V_a}{k_{VB}}\right) \tag{10}$$

which bears strong similarity to the way pentode anode currents are modelled. From Eq. (9), the second grid $g2$ is modelled as another control grid, as V_{g1} and V_{g2} are treated on equal footing. The third grid-current I_{g3} is modelled as:

$$I_{g3} = \frac{1}{k_{g2}} e^{x(\log(\frac{V_{g3}}{\mu} + (V_{g1}+V_{g2})))} \tag{11}$$

which bears resemblance to the screen grid current Eq. (8) for the Koren pentode model. Based on this observation and the observation that V_{g1} and V_{g2} are treated on equal footing, the question arises whether the second and third grid have been interchanged in the model. In most, if not all, practical applications, $g3$ is used as a control grid (in mixer applications this grid is connected to the oscillator output), and $g2$ and $g4$ are internally connected and (DC) stabilized at a specific voltage.

If the assumption is made that indeed $g2, g4$ and $g3$ are interchanged in the model, we are left with the fact that (as in the pentode case) $I_{g2,g4}$ is independent of the anode voltage V_a, which in practice is certainly not true.

3.4 Some issues with Koren's models

While Koren's models represent a substantial improvement over all prior modelling efforts, still a few known deficiencies exist. In this section we will investigate some of those.

3.4.1 Analysis of the Koren triode model

Experience by various users of the Koren model lead to the observation that mild differences in optimization method, with minute differences in fitting residual, could lead to sizeable differences in parameter values. It is therefore interesting to calculate the Hessian matrix of all second derivatives [PTVF92], and perform the eigenanalysis of the Hessian. Large eigenvalues will show that the parameters in the corresponding eigenvector have a big impact on the fitting residual, and, vice versa, small

eigenvalues will show what parameter combinations in the corresponding eigenvector will have little impact. An example is shown below, and represents the eigenanalysis of an ECC81 triode at the point of convergence:

```
 Eigen analysis of Hessian matrix:

 Eigenvalues:
         0.27E-03  0.23E-05  0.48E-09 -0.45E-10  0.72E-13
 Eigenvalues normalized:
         0.10E+01  0.84E-02  0.18E-05 -0.17E-06  0.27E-09

 Eigenvectors:

mu        -0.0442    0.9924   -0.0444   -0.1064    0.0007
ex         0.9990    0.0443   -0.0028   -0.0001    0.0001
kG1       -0.0045    0.0775   -0.4239    0.9023    0.0090
kp        -0.0012    0.0852    0.9045    0.4177   -0.0080
kVB        0.0000   -0.0007    0.0111   -0.0048    0.9999
```

A number of observations can be made based on this analysis:

1. The third and fourth largest eigenvalues show that the parameters k_G and k_p are not orthogonal, and, more importantly, especially the fourth eigenvalue hardly contributes to the fitting result. This means that k_{G1} could vary substantially, if kp would change concommittantly, without affecting the model values. In other words, k_G and k_p fulfill the same role in the model; and having two parameters for the same role could easily lead to over-fitting. This is potentially harmful, as this may lead to fitting non-physical effects like noise. Also it means that it makes no sense comparing different triodes based on their values for k_{G1} and k_p.

2. The smallest eigenvalue corresponds almost uniquely to the parameter k_{VB}. This means that leaving out the parameter k_{VB} would have had little or no impact on the fitting residual. This is understandable, because k_{VB} describes the 'island' effect which only plays a role at very low anode currents. The fact that the eigenvalue is associated uniquely with k_{VB} shows that the fit will also not be 'over-parametrized'. In other words, leaving k_{VB} in the model may not help in this case, but also does not harm.

3. The parameters μ and x are pretty unique, and have a big impact on the curve shape. Nevertheless, there is some degree of correlation between these parameters, which means that small changes in μ can be compensated for by small changes in x without affecting the model values too much.

As long as there is no alternative to the Koren model, it will remain the basis of many (good) Spice models. However, it is flawed, as is demonstrated by the first item in the previous discussion[1].

3.4.2 Triode strapped pentodes

Often one would like to use a pentode in triode connection, *i.e.*, the screen grid is connected to the anode, and the total anode current $I_{\mathrm{a,pseudo}}$ for this pseudo-triode is given by:

[1] Recently, the author has been made aware of the existance of new work by Adrian [Adr14]. In this work new triode and pentode models are derived, which are claimed to be more robust compared to Koren's models.

$$I_{\mathrm{a,pseudo}} = I_a(V_a, V_a, V_g) + I_{g2}(V_a, V_g) \tag{12}$$

demonstrating that anode and screen voltages are equal. From the expressions for anode and screen currents, Eq. (7) and Eq. (8) respectively, one can see that this model predicts a scaling behaviour for $I_{\mathrm{a,pseudo}}$ which is very different from the scaling behaviour for a triode (Eq. (5)). A similar observation can be made with respect to the extension of the Koren model to heptodes (see Sec. 3.3). The next section Sec. 4 seeks to remedy this inconsistency.

4 New pentode model

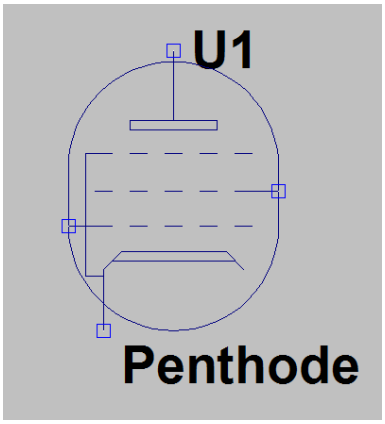

Figure 3: Pentode symbol (created in LTSpice) representing the model development in Sec. 4. The suppressor grid g3 is tied to the cathode.

A fundamental problem the Koren pentode model has is that a pentode model, wired as a triode, will by construction behave differently as when it where described by a triode model. This inconsistency will be addressed by the definition of what hence forth will be called the 'Koren current'. Note, that as in Koren's original model, the fundamental assumption is made that the suppressor grid g_3 always is at zero potential, and therefore its influence is not modelled separately.

4.1 Definition of 'Koren current' $I_{P,Koren}$

In the Koren model for pentodes, Koren simplifies the equation Eq. (4)for his potential $E_{1,T}$ for triodes:

$$E_{1,T} = \frac{V_p}{k_p} \log\left(1 + e^{(k_p(1/\mu + V_g/\sqrt{k_{VB}+V_a^2}))}\right) \tag{13}$$

to Eq. (6),

$$E_{1,pentode} = \frac{V_{g2}}{k_p} \log\left(1 + e^{(k_p(1/\mu + V_g/V_{g2}))}\right)$$

without further rationale. A rationale might be computational efficiency (which in 2001 could have been a perfectly valid reason) for this simplification. As a pentode model, strapped as a triode, should give an equally good fit as the triode model of the actual pentode in triode mode, this simplification has not been taken over in the new models presented below. In the next sections the following definition for what we will call the 'Koren current' $I_{P,Koren}$ will be used:

$$I_{P,Koren}(V_{g2}, V_g) = \frac{1}{2} E_{1,p}^x (1 + \mathrm{sgn}(E_{1,p})) \tag{14}$$

$$E_{1,p} = \left(\frac{V_{g2}}{k_p}\right) \log\left(1 + e^{k_p(1/\mu + V_g/\sqrt{k_{VB}+V_{g2}^2})}\right) \tag{15}$$

It is important to note that this definition of the current does not include any scaling parameter k_{g1} or k_{g2}. In subsequent references to $I_{P,koren}(V_{g2}, V_g)$, for notational convenience the explicit dependency on V_{g2}, V_g may get dropped, and reference is simply made to $I_{P,koren}$.

4.2 New Koren pentode model

With the definition of the Koren current, we can now write for the anode and screen currents:

$$I_a(V_{g2}, V_g) = \frac{I_{P,Koren}}{k_{G1}} \arctan\left(\frac{V_a}{k_{VB}}\right) \tag{16}$$

and

$$I_{g2}(V_{g2}, V_g) = \frac{I_{P,Koren}}{k_{g2}} \tag{17}$$

While this may improve the quality of the fit of (especially) the screen current, it still does not give consistency between a triode and a pentode, wired as triode, model.

4.3 Constant Space Charge

For pentodes, the concept of constant space charge is both experimentally and theoretically well underpinned [Spa48]. This concept is based on the fact that the total space charge, and hence total cathode current, is independent of V_a for a given screen voltage V_{g2} - see App A for examples. It is clear that the Koren pentode models (both the original as well as the new) do not display the effect of constant space current, as the anode current shows a dependency on V_a, V_{g2}, and the screen current does not. In this section we will define a model for the description of the total current $I_a + I_{g2}$. A key assumption of the concept of constant space charge is that the 'Durchgriff' D_a of the anode is zero, in other words, anode voltage variations have no impact on the cathode current (or total space current). It appears that for small signal pentodes this assumption is largely true. For power pentodes (and beam tetrodes) however D_a is non-zero. *I still need to figure out why.* From practical observations it appears that the effect of anode voltage variations is almost linear. We will account for this effect by a factor AV_a. At very low anode voltages, the total space charge current is reduced slightly. Hence, ignoring the small decrease in current at low anode voltages, the expression for the total space current (or, equivalently, the cathode current I_c) now becomes:

$$I_c(V_a) = I_a(V_a) + I_{g2}(V_a) = \frac{I_{P,Koren}}{k_{g_1}}(1 + AV_a) \tag{18}$$

Note, that by construction, this gives a pseudo anode current for a triode-strapped pentode which is very close to the triode anode current scaling. Only if $|A|$ substantially deviates from zero, there is still a dissimilarity between the triode scaling, and the results obtained by adding anode and screen currents. This discrepancy can by quantified by examining the behaviour of Eq. (18) for large values of V_a. in that case we can approximate $I_c(V_a)$as

$$I_c(V_a) \approx \frac{1}{k_{g1}}(\frac{V_a}{\mu} + V_{g1})^x(1 + AV_a) \tag{19}$$

which we now seek to write as a triode anode current, where all parameters except the exponent x remain identical:

$$I_c(V_a) \approx \frac{1}{k_{g1}}(\frac{V_a}{\mu} + V_{g1})^{(x+\delta x)} \tag{20}$$

which implies we seek a δx such, that

$$(1 + AV_a) \approx (\frac{V_a}{\mu} + V_{g1})^{\delta x} \tag{21}$$

As we make the assumption of $V_a = V_{a,\max}$ being very large, we can thus approximate δx as

$$\delta x \approx \ln(1 + AV_{a,\max})/\ln(\frac{V_{a,\max}}{\mu}) \tag{22}$$

where for all practical case we take $V_{a,rmmax} = 500V$ (note thatthe precise value of this voltage is not very critical). For $A = 0$, we clearly have $\delta x = 0$ as it should be, and correspondence between the triode model and pentode model is absolute. For cases where A substantially deviates from zero, as in many power pentodes, the triode parameters are equal to those in the pentode model, except for the deviation δx as described by Eq. (22). In versions of the models disseminated in `TubeLib.inc` before June 2015, this correction δx was not included in the triode models. However, for some pentodes this could give rise to about a 10% difference in anode currents for the triode model and the pentode models (with anode and g2 connected). With the correction included, this difference is reduced to about 1%.

In the following sections the notion of constant space current will be further exploited.

4.4 Screen and anode currents I

From Appendix B.1 we see that an expected scaling relation for the screen current is to be inversely proportional to the anode voltage plus a constant. This is clearly only valid in case secondary emission is not relevant, and true for most small signal pentodes. We will hence write a scaling law for the screen current as:

$$I_{g2}(V_a) = \frac{I_{\mathrm{P,Koren}}}{k_{g_2}}(1 + \frac{\alpha_s}{(1+\beta V_a)}) \tag{23}$$

With the concept of constant space current, this will allow us to obtain the anode current. A small refinement of Eq. (18) will be introduced.

At very low anode voltages, the total space charge is reduced slightly. We model that effect by subtracting a factor $\alpha/(1+\beta V_a)$ from the total space current - as will be shown later, α is not a fitting parameter. There is no physical underpinning for this approach - and because the reduction of space current is only very small, this approach, that does not introduce any new fitting parameters, has been chosen. It is amazing how accurate this model is, even in cases where secondary emission is very visible (see also App A). The expression for the total space charge current now becomes:

$$I_a(V_a) + I_{g2}(V_a) = \frac{I_{P,Koren}}{k_{g_1}}(1 + AV_a - \frac{\alpha}{1+\beta V_a}) \tag{24}$$

For which the expression for the anode current now becomes:

$$I_a(V_a) = I_{\mathrm{P,Koren}}(\frac{1}{k_{g1}} - \frac{1}{k_{g2}} + \frac{AV_a}{k_{g1}} - \frac{1}{(1+\beta V_a)}(\frac{\alpha}{k_{g1}} + \frac{\alpha_s}{k_{g2}})) \tag{25}$$

Because the anode current should equal zero at zero anode voltage, we further have:

$$\frac{1}{k_{g1}} - \frac{1}{k_{g2}} = \frac{\alpha}{k_{g1}} + \frac{\alpha_s}{k_{g2}} \tag{26}$$

Hence

$$\alpha = 1 - \frac{k_{g1}}{k_{g2}}(1 + \alpha_s) \tag{27}$$

Showing that α is not an independent parameter. In the modeling program `ExtractModel` this model is named 'Derk' (see Sec. 13.1).

In Fig. 4 the model has been fitted to the same PF86 that was used to fit the model of Koren to. The description of the 'knee' at low voltages, and the screen current, are both excellent, and representative of similar fits to many other small signal pentodes (e.g. E(C)F80).

4.5 Screen and anode currents II

While for an 'ideal' pentode the screen current should be roughly inversely proportional to the anode voltage, this scaling behaviour is not always true as illustrated in Fig. 5 where on the left an EF80 is fitted with the pentode model developed in the previous section.

While the total cathode current is still pretty much constant except for very low anode voltages, the EF80 does not show the smooth anode current dependence on anode voltage. This phenomenon is well-known amongst the beam-tetrode advocates [Sch38], and is called 'critical compensation'. The rounded knee of a pentode is called 'over compensated' and results in a smaller region of operating in a linear $I_a - V_a$ regime. For the EF80, in particular the 'knee' is not well modeled; the EF80 data

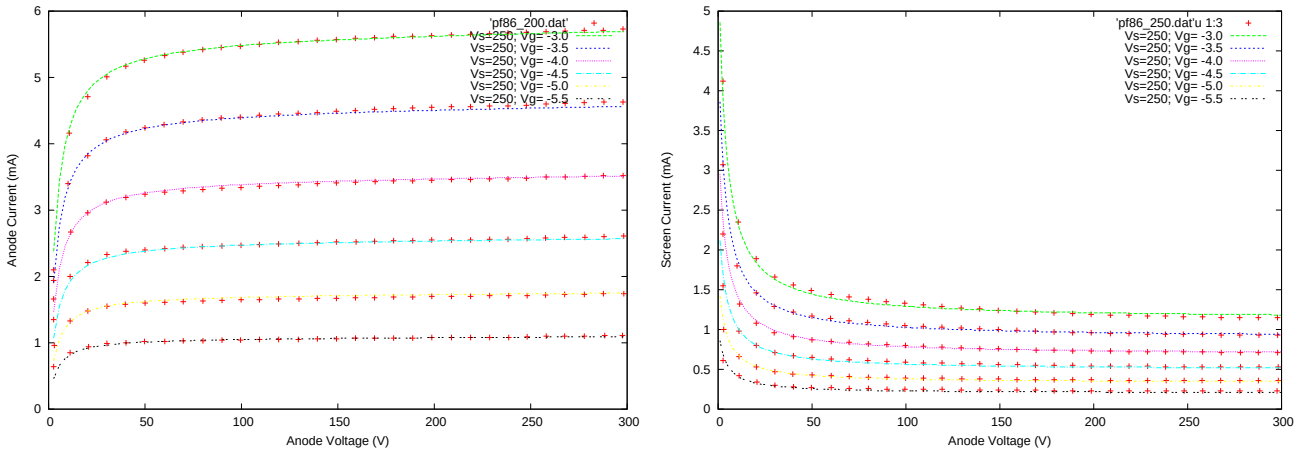

Figure 4: Model fits of anode and screen current of a PF86 according to the model of Sec. 4.4.

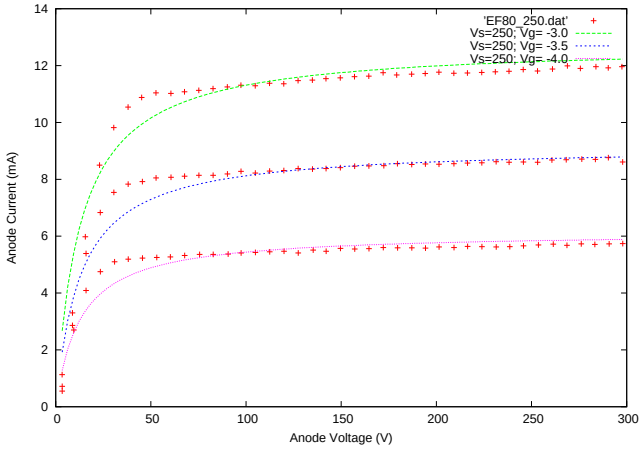

Figure 5: Model fits of anode current of a EF80 according to the model of Sec. 4.4.

show a rather sharp knee, as opposed to the smooth curve the EF86 presents. The origin in this lies in the fact that the EF80 behaves much like a beam tetrode does: see Appendix B.
From Appendix B, we will hence write a scaling law for the screen current as:

$$I_{g2}(V_a) = \frac{I_{P,Koren}}{k_{g2}}(1 + \alpha_s e^{(-\beta V_a)^{3/2}}) \tag{28}$$

With the concept of constant space current, this will allow us to obtain the anode current. As in Sec. 4.4, a small refinement of Eq. (18) will be introduced.

At very low anode voltages, the slight total space current reduction is modelled by subtracting a factor $\alpha e^{(-\beta V_a)^{3/2}}$ from the total space current. As in Sec. 4.4, α is not a fitting parameter. Also here is no physical underpinning for this approach - and has been chosen as it improves modelling while not introducing new fitting parameters. The expression for the total space charge current thus becomes:

$$I_a(V_a) + I_{g2}(V_a) = \frac{I_{\mathrm{P,Koren}}}{k_{g1}}(1 + AV_a - \alpha e^{(-\beta V_a)^{3/2}}) \tag{29}$$

As a result, the anode current Ia now is given by:

$$I_a(V_a) = I_{\mathrm{P,Koren}}(\frac{1}{k_{g1}} - \frac{1}{k_{g2}} + \frac{AV_a}{k_{g1}} - e^{(-\beta V_a)^{3/2}}(\frac{\alpha}{k_{g1}} + \frac{\alpha_s}{k_{g2}})) \tag{30}$$

Because the anode current should equal zero at zero anode voltage, we further have as in the first pentode model:

$$\frac{1}{k_{g1}} - \frac{1}{k_{g2}} = \frac{\alpha}{k_{g1}} + \frac{\alpha_s}{k_{g2}} \tag{31}$$

Hence

$$\alpha = 1 - \frac{k_{g1}}{k_{g2}}(1 + \alpha_s) \tag{32}$$

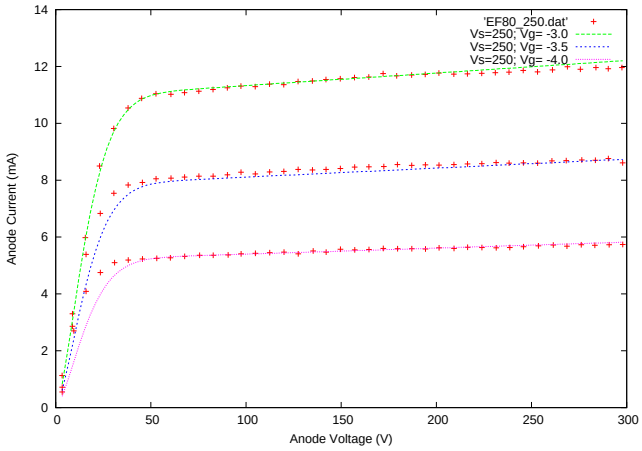

Figure 6: Model fits of anode current of a EF80 according to the model of Sec. 4.5.

A fit of this model to the same EF80 data as discussed previously is shown in Fig. 6. Especially for low grid voltages, the knee is still not perfectly represented; and further work is needed. The fit is much better however compared to the original model. In ExtractModel, this model is called 'DerkE'.

4.6 Pentode model choice

A first choice to be made is whether or not to stick to the (modified) Koren model. This model has its simplicity as a clear advantage over the Derk(E) models. In Spice simulations however, it appears that simulation time is hardly affected by the choice of the model; hence the more elaborate new models are to be preferred. As a next step, the choice between the two new models needs to be made. For real beam tetrodes, lacking a 3rd grid and having focussing electrodes instead, this usually is mentioned in the datasheet. Typically these will be power tubes. For small signal tubes, it is often not mentioned in the datasheet whether a pentode is a pure pentode, or a beam-like pentode (real beam tetrodes in small signal applications are rare). Visual inspection often gives a clue, as pentodes with a circular anode are all 'real' pentodes. pentodes that have 2 small stripes of metal as anode can behave as a beam pentode. However, it still depends on how the (screen and suppressor) grids are aligned with respect to each other. If all the grids are aligned, chances are high it is a beam pentode. Investigation of the voltage-current behaviour at low anode voltages will provide the answer in all cases.

5 Variable-mu pentodes

Variable-mu pentodes (or, remote cut-off pentodes) have specifically been designed to have a very non-linear behaviour. This behaviour allows to operate the tube at very negative grid voltages V_{g1}, where the steepness of the $I_a - V_a$ curves is reduced compared to the steepness at moderate values

of V_{g1}. As a result, the amplification at highly negative grid voltages is substantially reduced. This behaviour is demonstrated in Fig. 7 where the non-linear behaviour is clearly visible.

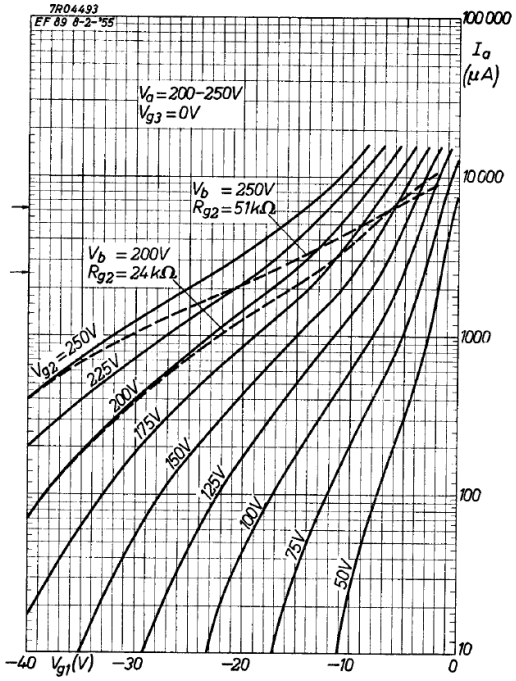

Figure 7: Anode current of the EF89 according to the Philips datasheet.

The Koren current would result in rather linear behaviour, and definitely not display the typical 'kink' as observed in the curves of Fig. 7. In order to assess the severity of this shortcoming, it was tried to fit the data of a 6K7 strapped as a triode, to the Koren triode model. The result is shown in Fig. 8.

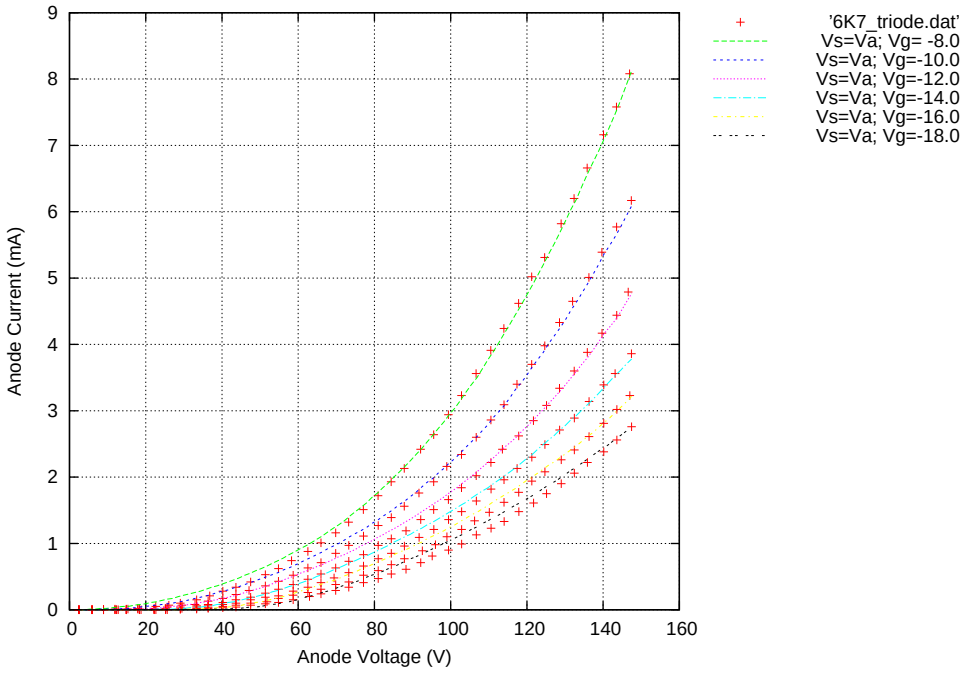

Figure 8: Triode fit of a 6K7 variable mu pentode, strapped in triode mode. Visible is a rather structural mis fit of the data.

The fit is of poor quality, showing structural fitting problems for more negative grid voltages, but also at low anode voltages at moderate grid voltages. Given the fact that usually the Koren triode model typically is capable of providing a very good fit, this is a remarkable observation. Moreover, the fit as displayed resulted in an unphysically high mu value of well over 1000. Restricting the value of μ to a more realistic value resulted in a significantly worse fit, leading to the conclusion that a new model is required to describe the characteristics of a variable-mu pentode.

In a practical realization of a variable-mu pentode, the required non-linear behaviour is created by varying the gridwire spacing of the first grid - typically the spacing would be small at the top and the bottom of the tube assembly, and have a larger large spacing in the middle. A simplified view therefore could be to view the variable-mu pentode as two separate pentodes in parallel, one characterised by a large grid spacing, and one by a small spacing. As in practice there is a very gradual transition between the two extreme gid spacings (the one at the top/bottom of the tube, and the one in the middle) this is clearly a simplification. In the following sections the model based on this assumption will be derived and results tested.

5.1 Variable-mu pentode models

Based on the assumptions described in the prior, we will model a variable-mu pentode as two pentodes in parallel, each with their own Koren currents $I_{\mathrm{P,Koren}_a}$ and $I_{\mathrm{P,Koren}_b}$:

$$I_{\mathrm{P,Koren}_v} = (1 - s_{\mathrm{var}}) I_{\mathrm{P,Koren}_a} + s_{\mathrm{var}} I_{\mathrm{P,Koren}_b} \tag{33}$$

where $I_{\mathrm{P,Koren}_v}$ is the effective, net Koren current. The fraction s_{var} determines the relative contribution of the different constituting Koren currents, and therefore we have $0 \leq s_{\mathrm{var}} \leq 1$. The Koren currents $I_{\mathrm{P,Koren}_a}$ and $I_{\mathrm{P,Koren}_b}$ are defined *cf.* Sec 4.1 as:

$$I_{P,Koren_a}(V_{g2}, V_g) = \frac{1}{2}(E_{1,p})_a^{x_a}(1 + \mathrm{sgn}((E_{1,p})_a)) \tag{34}$$

$$(E_{1,p})_a = (\frac{V_{g2}}{k_p}) \log\left(1 + e^{k_p(1/\mu_a + V_g/\sqrt{k_{VB}+V_{g2}^2})}\right) \tag{35}$$

and likewise for $I_{\mathrm{P,Koren}_b}$. Note that with this definition, the discrimination between the different currents is determined by the 'amplification factor' $\mu_{a,b}$ and the exponent $x_{a,b}$. The other factors k_p and k_{VB} are taken identical for both currents. These factors are largely determined by geomety, which very likely will be rather identical for both parallel pentodes. The only exception might be in the island effect, which might be different based on the different grid spacings. However, experience so far is that this does not significantly limit the accuracy of the modelling.

Using this approach, we follow the reasoning in Sec. 4.3, for determining the space charge current for a variable mu pentode. This leads to an expression very similar to the space charge current for a regular pentode, Eq. (24):

$$I_a(V_a) + I_{g2}(V_a) = \frac{I_{\mathrm{P,Koren}_v}}{k_{g_1}}(1 + AV_a - \frac{\alpha}{1 + \beta V_a}) \tag{36}$$

where $I_{\mathrm{P,Koren}_v}$ is given by Eq. (33).

We have identified in the previous sections that, for the description of the variety in different regular pentodes, two different models are required which were coined 'Derk' and 'DerkE', respectively. With the variable mu Koren current definition, the approach outlined in Sec. 4.4 can be followed for model 'Derk'. The screen current is hence described by:

$$I_{g2}(V_a) = \frac{I_{\mathrm{P,Koren}_v}}{k_{g_2}}(1 + \frac{\alpha_s}{(1 + \beta V_a)}) \tag{37}$$

and the expression for the anode current now becomes:

$$I_a(V_a) = I_{\mathrm{P,Koren}_v}(\frac{1}{k_{g1}} - \frac{1}{k_{g2}} + \frac{AV_a}{k_{g1}} - \frac{1}{(1 + \beta V_a)}(\frac{\alpha}{k_{g1}} + \frac{\alpha_s}{k_{g2}})) \tag{38}$$

Because the anode current should equal zero at zero anode voltage, we further have:

$$\frac{1}{k_{g1}} - \frac{1}{k_{g2}} = \frac{\alpha}{k_{g1}} + \frac{\alpha_s}{k_{g2}} \tag{39}$$

Hence

$$\alpha = 1 - \frac{k_{g1}}{k_{g2}}(1 + \alpha_s) \tag{40}$$

Showing that α is not an independent parameter. In the modeling program `ExtractModel` this model is named 'Derk' (see Sec. 13.1).

The approach to derive the 'DerkE' version will not be outlined here, but follows identical reasoning.

5.2 Variable-mu pentode models - results

In Fig. 9, typical results of the fit of the model described previously in Sec. 5.1 are shown. The fit is performed using the 'DerkE' model, as (especially at low screen voltages) the curves show a very pronounced kink at low V_a, resembling the behaviour of the EF80. Small effects of secondary emission are visible, especially at highly negative V_{g1}. For lower screen voltages these effects are less pronounced.

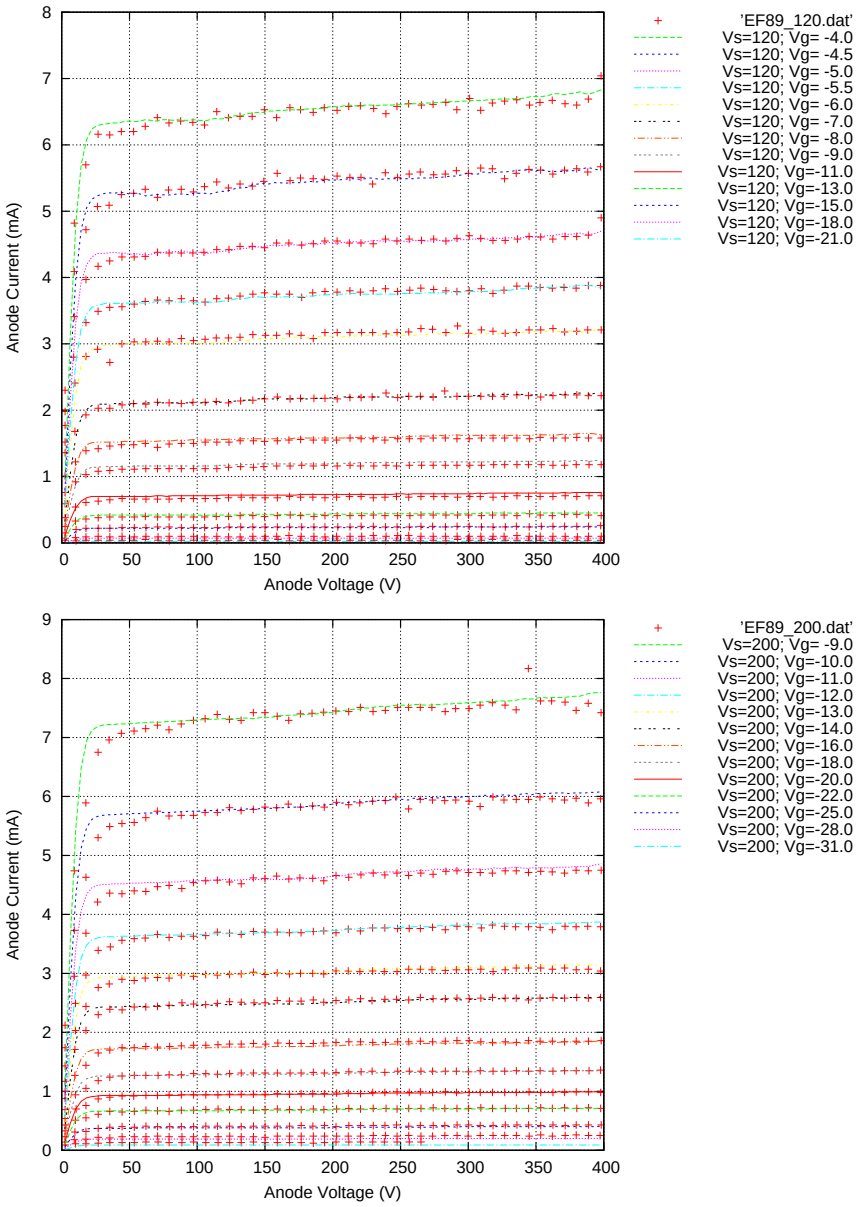

Figure 9: Fit of a EF89 pentode, using the 'DerkE' version of the model described in Sec. 5.1.

Overall, the fit is quite good, over a large range of grid voltages. The fitted values of $\mu_{a,b}$ differ by about a factor of 3.5, which seems to be rather typical for the (limited) set of variable-mu pentodes fitted so far. The relative contribution $s_{\rm var} \approx 0.05 - 0.1$ typically, where $\mu_a > \mu_b$. This is understandable, as a large fraction $s_{\rm var}$ would lead to a very high perveance - which is not desirable for a preamplifier.

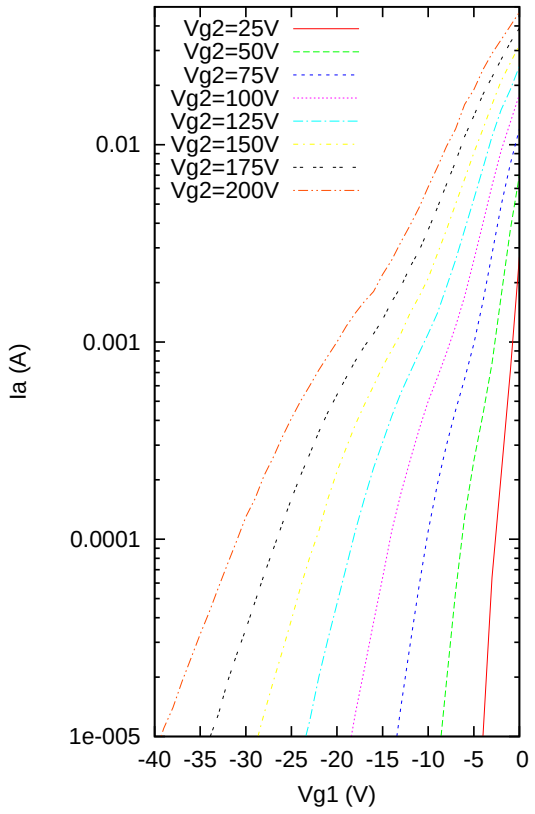

Figure 10: Based on the fit of a EF89 pentode, the non-linearity in the EF89 characteristics is visible and largely resembles that of Fig. 7.

In Fig. 10, model results for the EF89 are represented in a way identical to the representation in Fig. 7. The non-linear behaviour is well-described, and shows a gradual transition between the two different pentode behaviours around and anode current of about 2mA. The difference between the curves from the data sheet and those presented in Fig. 10 is primarily for high anode currents, where the model shows a less steep increase in current compared to the data sheet.

6 Secondary emission

In many power pentodes, and certainly power beam tetrodes, secondary emission of the anode is prominently present. The electrons emitted from the anode can get attracted to the screen in case the potential of the anode is lower than that of the grid. In this way there will be an effective decrease of the anode curent, and an equal increase in the screen current. secondary emission is an undesirable effect and is often not well represented in data sheets.

In Fig. 11, the $I_a - V_a$ and $I_{g2} - V_a$ curves from the Philips datasheet for the PL504 (identical to the EL500 except for the heater voltage/current) are shown. Hardly any effect due to secondary emission is visible in the anode current.

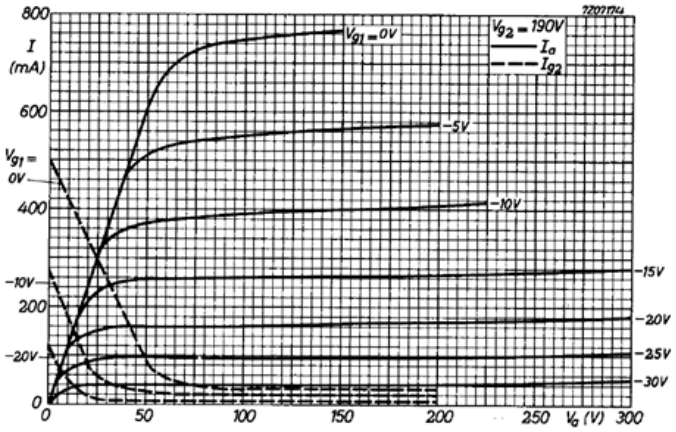

Figure 11: Anode current of a EL500/PL504 according to the Philips datasheet.

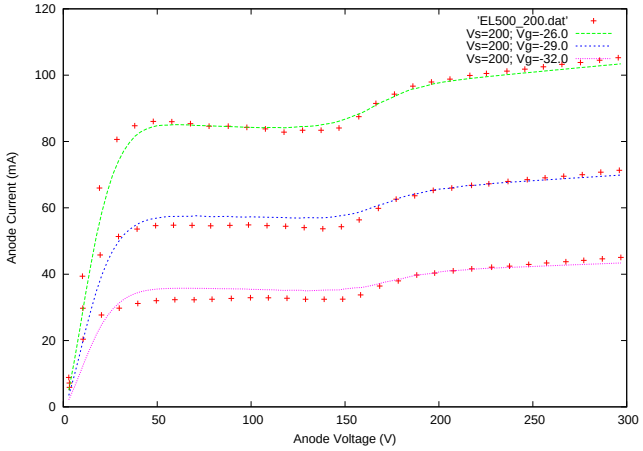

Figure 12: Anode current of a EL500/PL504 as measured with the uTracer. The drawn lines are fits based on the model presented in Sec. 6.4.

If the actual curves are measured however (see Fig. 12), there are very visible effects, that are not present in the curves in the datasheet. Note also that the screen currents are shown only for anode voltages lower than 200V, exactly where the most prominent effects due to secondary emission are expected. In its function as a TV line output tube, where the tube would spend most of its time at anode voltages well below 100V, the kinks induced by secondary emission are not relevant. In case secondary emission becomes important, the model describing the pentode needs to be updated.

6.1 Description of secondary emission effects

To describe the secondary emission effect on screen and anode currents, we will assume that the number of secondary emitted electrons is proportional to the energy of incident primary electrons on the anode (i.e. V_a). This assumption is underpinned by data in [Spa48], and data on the EL500 (see Fig 14) also demonstrate the linear dependency. At a certain voltage, the emitted electrons will no longer be attracted by the screen, but return to the anode. The voltage at which this happens will be dependent on the anode voltage, and the beam controlling voltages of the grids. As a result a descriptive form for the secondary emission current contribution to the space current can be written as:

$$P_{sec} = SV_a(1 + \tanh(-a_p(V_a - V_{\text{co}}))) \tag{41}$$

The first term SV_a describes the linear increase with anode voltage due to the increased impact energy of the primary electrons. The form $(1 + \tanh(-a_p(...)))$ is a phenomenological approximation to the complex function describing the cross-over region where the emitted electrons no longer get attracted by the screen, but return to the anode instead. The width of this cross-over region is described by the parameter a_p. Clearly the exact shape of this cross-over is a complex function of the exact geometry of the tube – but no attempt is made for a better description. The exact value of the cross-over voltage V_{co} is determined by the effectiveness of the suppression of the secondary electrons.

6.2 Position of cross-over voltage V_{co}

As the cross-over voltage V_{co} is determined by the effectiveness with which the secondary emission can be suppressed, it will depend on a number of variables:

1. The position and voltage of the suppressor grid / beam forming plates. In the analyses so far the assumption has been made that the grid/beam forming plates are at zero (cathode) potential. As a result there is only the geometrical influence left; and the impact on V_{co} will be constant. The impact will be characterized by a parameter $V_{\text{co}} \propto w$.

2. The effect of the space charge, and how effective it is in repelling secondary electrons. The space charge density is primarily determined by V_{g1}. Under the assumption that the effects of this is linear (which if the voltage excursions are small enough is always true according to the principle of Taylor expansion) this effect can be captured with a description $V_{\text{co}} \propto -\nu V_{g1}$. The minus sign is used because a $V_{g1} \approx 0$ will result in a high space charge density, and in effective secondary electron emission suppression (and hence, a low V_{co}). Conversely, a highly negative V_{g1} will result in a low space charge density and thus a high V_{co}.

3. The value of V_{g2}. Clearly, with a lower V_{g2}, less secondary electrons will leave the anode. This effect is approximately linear with V_{g2}. The energy distribution of the secondary electrons is very narrow (see Ref. [Spa48]), and the angular distribution of the secondary electrons is very large. Therefore the electron velocity components normal to the anode have an almost uniform distribution from zero to the maximum velocity. This effect will be captured with a description $V_{\text{co}} \propto V_{g2}/\lambda$.

The position of the cross-over is hence described by $V_{\text{co}} = (V_{g2}/\lambda - \nu V_{g1} - w)$. Practice shows that ν typically varies between 1 to 4, and that for beam tetrodes $\lambda \approx 1$. For pentodes (with a suppressor grid) λ is typically much larger, upto about 20. This effect is logical, as for pentodes the screen is 'screened' by the suppressor grid.

The full description for the secondary emission effect now becomes:

$$P_{sec} = SV_a(1 + \tanh(-a_p(V_a - (\frac{V_{g2}}{\lambda} - \nu V_{g1} - w)))) \tag{42}$$

which will be used in the next sections.

6.3 Pentodes and secondary emisssion

With this description of the secondary current, we now have for a pentode that displays secondary emission:

$$I_{g2}(V_a) = \frac{I_{\mathrm{P,Koren}}}{k_{g2}}(1 + \frac{\alpha_s}{1 + \beta V_a} + P_{\mathrm{sec}}) \tag{43}$$

Because the concept of constant space current still holds, we thus have:

$$I_a(V_a) = I_{\mathrm{P,Koren}}(\frac{1}{k_{g1}} - \frac{1}{k_{g2}} + \frac{AV_a}{k_{g1}} - \frac{P_{\mathrm{sec}}}{k_{g2}} - \frac{1}{1 + \beta V_a}(\frac{\alpha}{k_{g1}} + \frac{\alpha_s}{k_{g2}})) \tag{44}$$

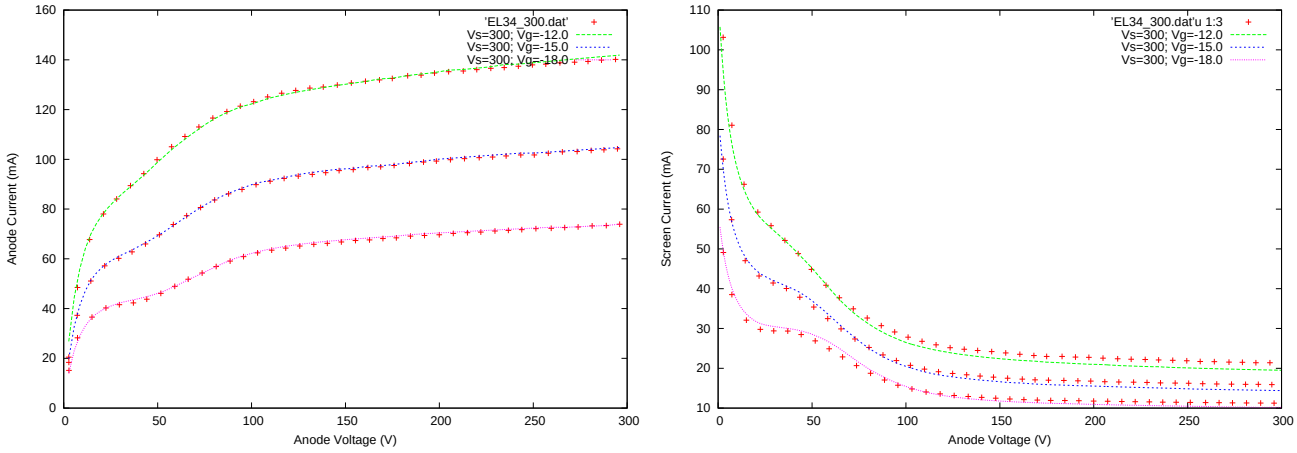

Figure 13: Model fits of anode and screen current of a EL34 according to the model of Sec. 6.3.

Above, results are shown for the beloved EL34 with a screen voltage of 300V, where the parameter fit was over $V_{g2} = 200, 250$, and 300V. While the secondary emission effects are only small, it still impacts the tube characteristics in an area that would be exercised at high current/voltage swings (*e.g.* in class B or AB). It is also worth to note that fitting this model with the beam tetrode model (see next section 6.4) gives substantially worse fitting results, confirming that the EL34 is a true pentode.

6.4 Beam tetrodes and secondary emission

Adding secondary emission to the tetrode model, we now have for the screen current:

$$I_{g2}(V_a) = \frac{I_{\mathrm{P,Koren}}}{k_{g2}}(1 + \alpha_s e^{-(\beta V_a)^{3/2}} + P_{\mathrm{sec}}) \tag{45}$$

From the concept of constant space we thus have:

$$I_a(V_a) = I_{\mathrm{P,Koren}}(\frac{1}{k_{g1}} - \frac{1}{k_{g2}} + \frac{AV_a}{k_{g1}} - \frac{P_{\mathrm{sec}}}{k_{g2}} - e^{-(\beta V_a)^{3/2}}(\frac{\alpha}{k_{g1}} + \frac{\alpha_s}{k_{g2}})) \tag{46}$$

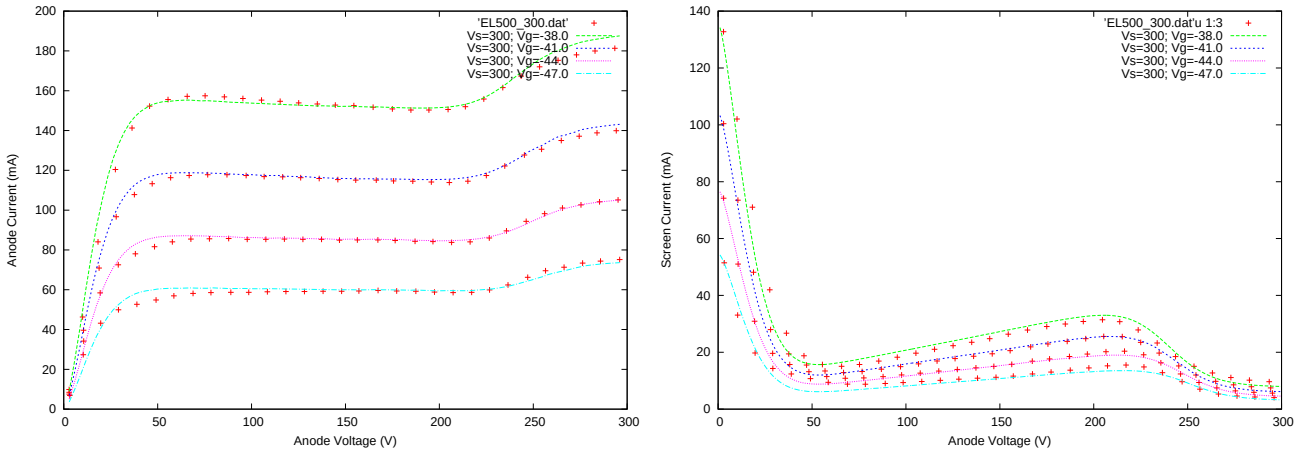

Figure 14: Model fits of anode and screen current of a EL500 according to the model of Sec. 6.4.

In Fig. 14, data is shown for the EL500 (identical to the PL504). This tube very nicely demonstrates the linear increase in secondary emission with anode voltage, due to the higher impact energy of the incident electrons. Although it is called a pentode in the Philips datasheets, it really is a beam tetrode. Fitting this tube with the pentode model will give inferior results. This tube exhibits very strong effects due to secondary emission; tubes designed for audio purposes will never have these huge effects. While the fit is not perfect, it captures all the important elements. The fitting errors are substantially smaller than the tube-to-tube variations.

7 Hexodes and heptodes

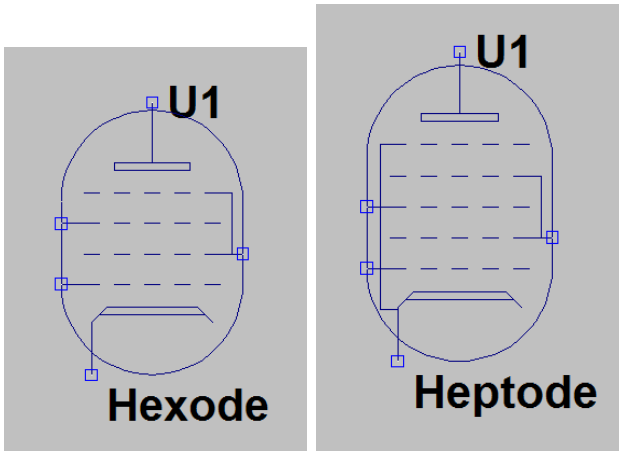

Figure 15: Left: Hexode symbol (created in LTSpice) representing the model development in Sec. 7. Right: the corresponding heptode symbol.

Hexodes and heptodes are important tubes in radio (and, to a lesser extent, in TV) history, and therefore deserve to be modeled. In this section, a hexode and heptode modeling will be derived, under the following assumptions:

1. For a heptode, the 5'th grid will be connected to the cathode;

2. For both heptodes as hexodes, the 2'nd and 4'th grid are connected. The grids will act as screen and/or accelerator grids, *i.e.*, have a high positive voltage and carry substantial current;

3. g1 will act as primary control grid; g3 acts as secondary control grid. Both control grids will have a negative potential (*i.e.*, carry little or no current).

The first two of these premises are also depicted in Fig. 15. The last prerequisite implies that the tube will be viewed as a pentode (or, in fact tetrode), consisting of the cathode, first grid, and 2nd (screen) grid; and stacked is a pentode (or tetrode for a hexode) with g3 as control grid, and g4 as screen grid.

7.1 Constant space current

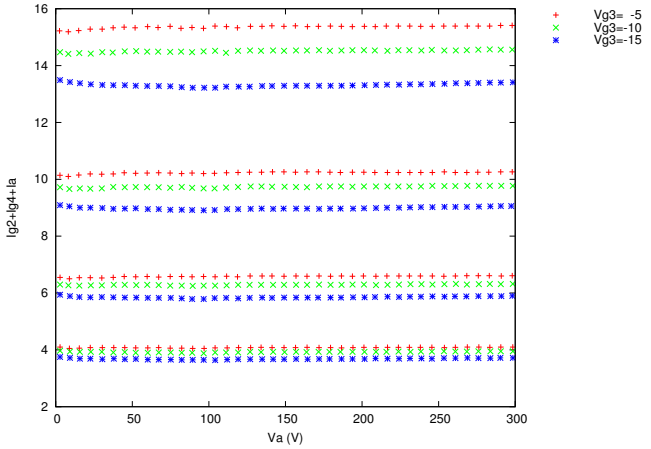

Figure 16: Space current for an ECH81 at $V_{g2} = V_{g4} = 100V$, for $V_{g1} = 1, 2, 3, 4$.

The concept of constant space current proves to also largely hold for heptodes. This is illustrated in Fig. 16 where space currents are shown for constant g_2 and g_4 voltage. Clearly the large number of grids creates perfect independence of the anode voltage for the total current! The A parameter is indistinguishable from zero, and the small influence V_{g3} still has on total current has is illustrated.

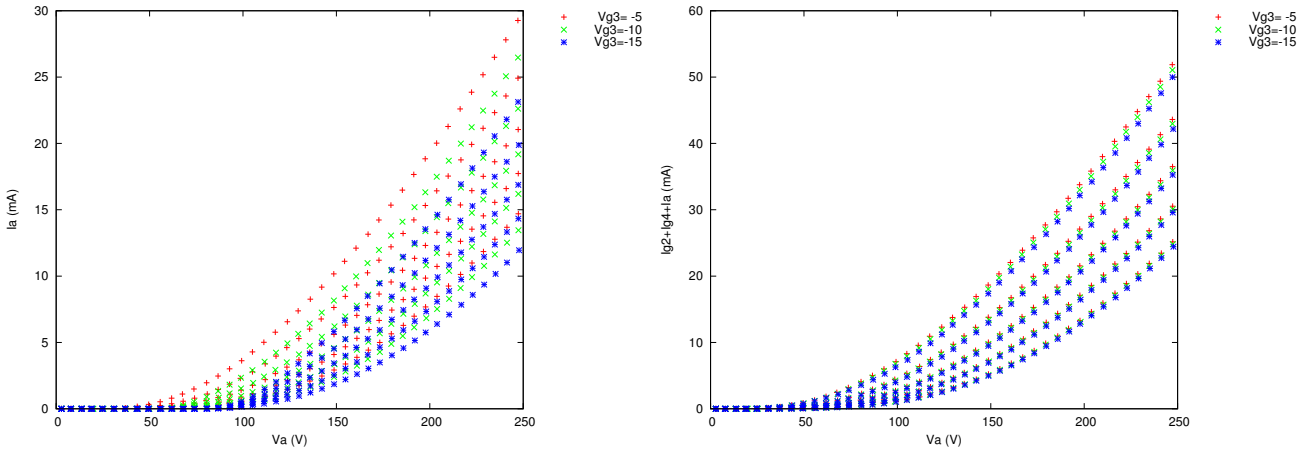

Figure 17: Left: Anode current I_a for an ECH81, with $V_a = V_{g2} = V_{g4}$, and for $V_{g1} = -2, -3, -4, -5, -6V$. Right: the same, but for the total space current $I_a + I_{g2} + I_{g4}$.

The implications of constant space current are further illustrated in the right of Fig. 17, where the space current of an ECH81 is displayed as function of V_a, for various values of V_{g3}. Clearly, the cathode current hardly depends on V_{g3}, consistent with the behaviour in Fig. 16, whereas V_{g1} is very influential on the total current. The fact that the ECH81 is a remote cut-off tube (*i.e.*, a variable grid spacing for g_1) is nicely demonstrated by the slowly increasing current at low anode voltages, rather than the rather abrupt increase in current normally observed in triodes.

That the *anode* current is dependent on V_{g3} is demonstrated by the left of Fig. 17. The anode current displays a dependency on V_a which is very similar to that of a regular triode, with the g3 as control grid.

Taking a similar approach as in Secs. 4.3 and 4.4, the total space current I_c is not (or hardly) dependent on V_{g3} or V_{g4}, and is written as:

$$I_c = I_a(V_a) + I_{g2}(V_a) + I_{g4}(V_a) = \frac{I_{H,1}}{k_{g_1}}(1 + AV_a - \frac{\alpha}{1+\beta V_a}) \tag{47}$$

Fig. 16 illustrates that the A parameter is virtually indistinguishable from zero, as is α. To maintain consistent with the pentode model, however, these parameters will remain included. As in the pentode case, α is not an independent parameter. We hence write:

$$I_{H,1}(V_{g2}, V_{g1}) = \frac{1}{2}E^x_{1,h}(1 + \mathrm{sgn}(E_{1,h})) \tag{48}$$

$$E_{1,h} = (\frac{V_{g2}}{k_p}) \log\left(1 + e^{k_p(1/\mu + (V_{g1}+V_{g3}/\mu_3)/\sqrt{k_{VB}+V^2_{g2}})}\right) \tag{49}$$

While there is a dependency on V_{g3} included in Eq. (49), Fig. 17 shows that this dependency is very small - in other words, μ_3 is very large. In subsequent references to $I_{PH,1}(V_{g2}, V_{g1})$, for notational convenience the explicit dependency on V_{g2}, V_{g1} may get dropped, and reference is simply made to $I_{H,1}$.

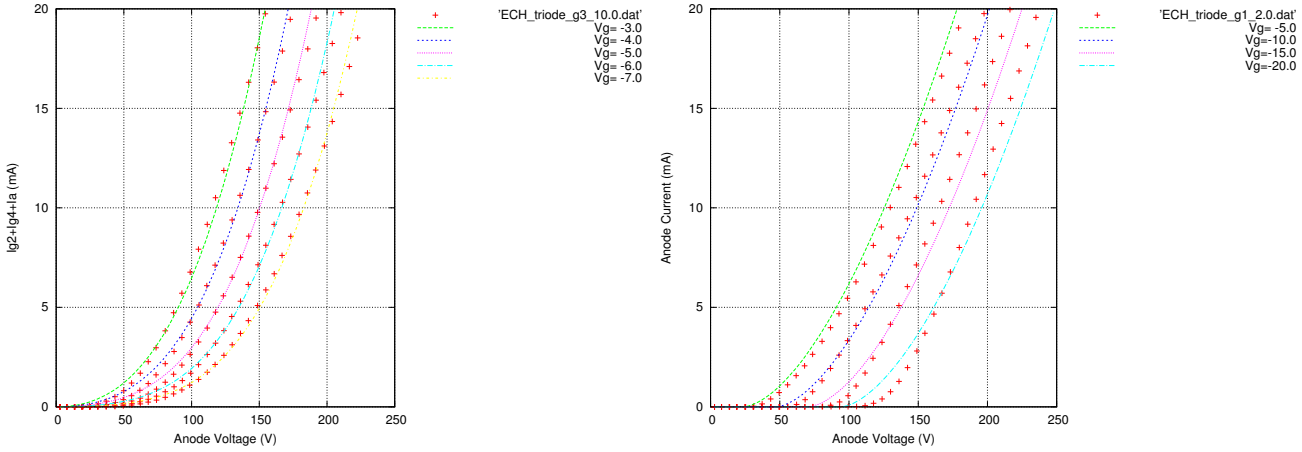

Figure 18: Left: Standard triode fit with $g1$ as control grid of total space current I_c at $V_{g3} = -10V$. Right: Standard triode fit with $g3$ as control grid of the anode current at $V_{g1} = -2V$.

The accuracy of this description for the total space current is illustrated in the left of Fig. 18, where a fit is displayed of Eq. (48) to the cathode current. For very high currents, the fit is not perfect, which is due to the fact that the tube starts to saturate at those currents. The ECH81 is only rated or cathode currents of 12.5mA maximum.

7.2 Anode and g2,g4 currents

We will model the heptode as a pentode, consisting of the cathode, g_1 as control grid, and g_2 as screen grid, with a pentode stacked on top of that. The mazes of g_2 replace the cathode in this model, g_3 becomes the control grid, and g_4 is the screen. The heptode anode is thus the pentode anode.

$$I_{H,2}(V_{g4}, V_{g3}) = \frac{1}{2} E_{2,h}^{x'}(1 + \mathrm{sgn}(E_{2,h})) \tag{50}$$

$$E_{2,h} = (\frac{V_{g4}}{k'_p}) \log\left(1 + e^{k'_p(1/\mu' + V_{g3}/\sqrt{k'_{VB} + V_{g4}^2})}\right) \tag{51}$$

As the upper grids $g3, g4$ and the anode form a pentode, with the electron source the mazes of the $g2$ grid that allow the electrons to pass, the pentode equation Eq. (25) can be used to describe the anode current. In Fig. 14, the anode current is displayed for a heptode strapped as triode. This behaviour should therefore be well described by:

$$I_a = I_{H,1}(\frac{1}{k_{g1}} - \frac{1}{k_{g2}} + \frac{AV_a}{k_{g1}} - \frac{1}{1+\beta V_a}(\frac{\alpha}{k_{g1}} + \frac{\alpha_s}{k_{g2}}))I_{H,2}(\frac{1}{k'_{g1}} - \frac{1}{k'_{g2}} + \frac{A'V_a}{k'_{g1}} - \frac{1}{1+\beta' V_a}(\frac{\alpha'}{k_{g1}} + \frac{\alpha'_s}{k'_{g2}}))$$

In all heptodes, the 2nd and 4th grid are connected. It is therefore not possible to easily distinguish the behaviour of the first pentode (tetrode) reflected by

$$(\frac{1}{k_{g1}} - \frac{1}{k_{g2}} + \frac{AV_a}{k_{g1}} - \frac{1}{1+\beta V_a}(\frac{\alpha}{k_{g1}} + \frac{\alpha_s}{k_{g2}}))$$

from the equivalent expression for the second pentode (tetrode):

$$(\frac{1}{k'_{g1}} - \frac{1}{k'_{g2}} + \frac{A'V_a}{k'_{g1}} - \frac{1}{1+\beta' V_a}(\frac{\alpha'}{k_{g1}} + \frac{\alpha'_s}{k'_{g2}}))$$

Therefore, the following approximation is made:

$$(\frac{1}{k'_{g1}} - \frac{1}{k'_{g2}} + \frac{A'V_a}{k'_{g1}} - \frac{1}{1+\beta' V_a}(\frac{\alpha'}{k_{g1}} + \frac{\alpha'_s}{k'_{g2}})) \approx \frac{1}{k'_{g1}}$$

where all impact of the 2nd and 4th grid is lumped together, leading to

$$I_a = I_{H,1}(\frac{1}{k_{g1}} - \frac{1}{k_{g2}} + \frac{AV_a}{k_{g1}} - \frac{1}{1+\beta V_a}(\frac{\alpha}{k_{g1}} + \frac{\alpha_s}{k_{g2}}))\frac{I_{H,2}}{k'_{g1}} \tag{52}$$

Because the anode current should equal zero at zero anode voltage, we further have as in the pentode case:

$$\frac{1}{k_{g1}} - \frac{1}{k_{g2}} = \frac{\alpha}{k_{g1}} + \frac{\alpha_s}{k_{g2}} \tag{53}$$

Hence

$$\alpha = 1 - \frac{k_{g1}}{k_{g2}}(1 + \alpha_s) \tag{54}$$

Showing that α is not an independent parameter. In the modeling program `ExtractModel` this model is named 'Derk' (see Sec. 13.1).

From the notion of constant space current we have

$$I_{g2,g4} = I_c - I_a$$

and thus

$$I_{g2,g4} = I_{H1,1}[\frac{1}{k_{g1}}(1 - \frac{I_{H,2}}{k'_{g1}} + \frac{I_{H,2}}{k'_{g1}}(\frac{1}{k_{g2}} - \frac{AV_a}{k_{g1}} + \frac{1}{1+\beta V_a}(\frac{\alpha}{k_{g1}} + \frac{\alpha_s}{k_{g2}}))] \tag{55}$$

7.3 Model results

In Fig. 19, the result if fitting the model described in the previous section to ECH81 data is displayed for a constant 2'nd and 4'th grid voltage of 150V. The tube displays a behaviour that is very similar to a regular pentode, and is well described by the model. Not shown here, is that for situations where the anode currents are substantially less than $I_{g2} + I_{g4}$, the fit may be inaccurately modelling the anode currents, mostly because of the fact that in a least squares fit $I_{g2} + I_{g4}$ will weigh much more if the anode currents are small. In general, errors are small compared to tube-to-tube variation. In testing 5 different ECH81 tubes, variation of anode current for the settings in Fig. 19 proved to be easily 20%, showing that with 5 grids, the manufacturing variations start to become very noticeable.

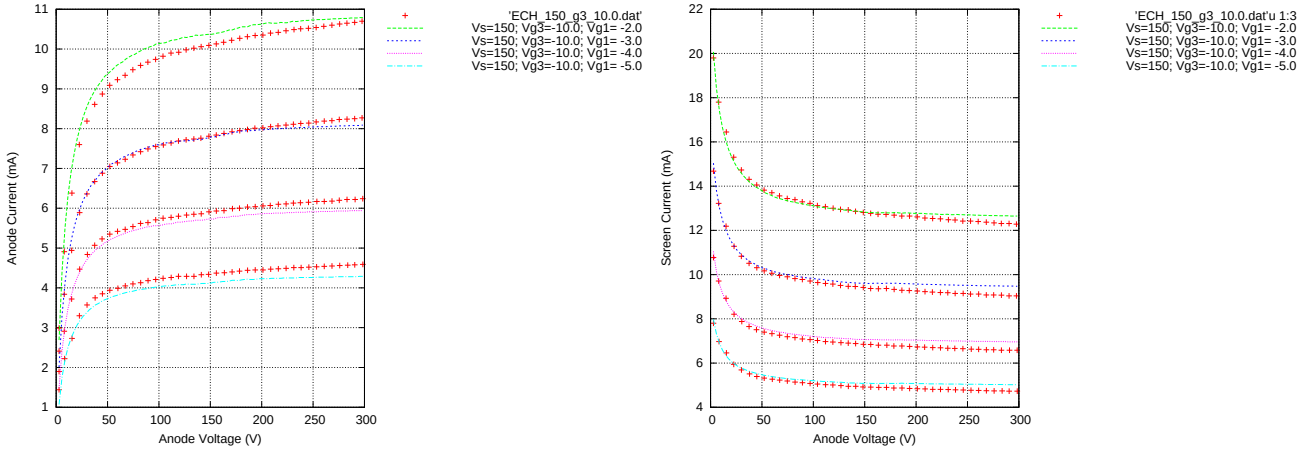

Figure 19: Left: Anode current I_a for an ECH81, with $V_{g2} = V_{g4} = 150V$, and for $V_{g1} = -2, -3, -4, -5V$. Right: the same, but for $I_{g2} + I_{g4}$.

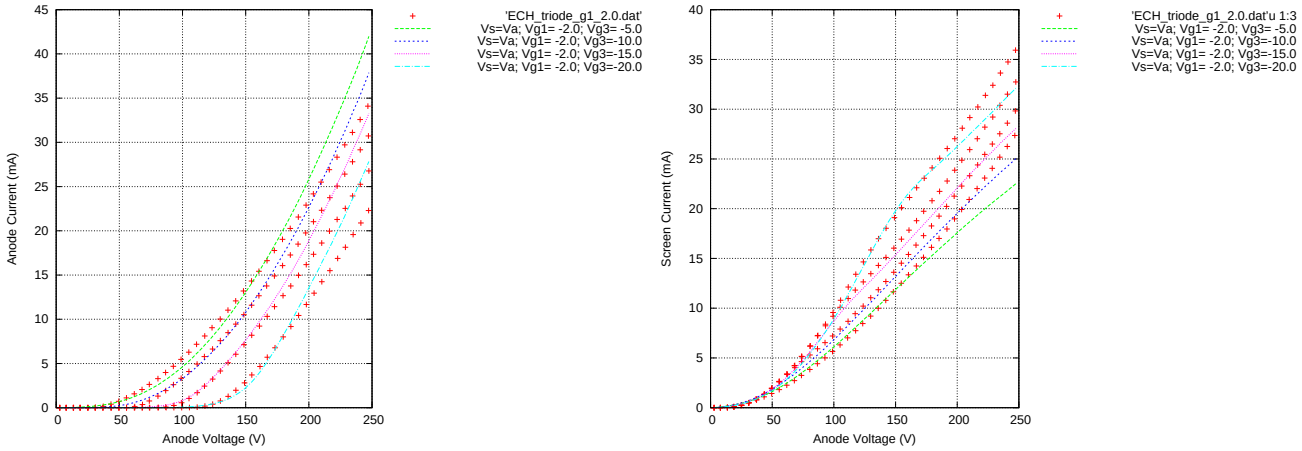

Figure 20: Left: Anode current I_a for an ECH81, with $V_a = V_{g2} = V_{g4}$, and for $V_{g3} = -5, -10, -15, -20V$. Right: the same, but for the total screen current $I_{g2} + I_{g4}$.

In Fig. 20 results are shown for a situation where $V_a = V_{g2,g4}$. This is not a practical situation, but illustrates nicely some aspects that set the heptode aside from a pentode. On the left in Fig. 20, the anode current for a ECH81 is shown as function of V_{g3}. The fit has been executed only for a anode power $P_a < 2W$, and the fit is quite dependent on that value. On the right $I_{g2,g4}$ is displayed. The effect of the constant space current is nicely visable. The screen current for $V_{g3} = -20V$ is the

highest, which is due to the fact that the current gets diverted to g_2. As the anode current suddenly increases as of $V_a = 150V$, there is a change in slope in the I_{g2g4} graph, due to the fact that current goes to the anode. As the fit is not perfect, the change in slope appears a bit too much. Further work will be needed to optimize the fitting procedure to correct for this. Nevertheless, the fact that the screen current for $V_a < 100V$ for $V_{g3} = -20$ and $V_{g3} = -15$ is identical, and only starts to diverge for $V_a > 100V$, is well modelled.

8 Pentode with separate g3 modulation

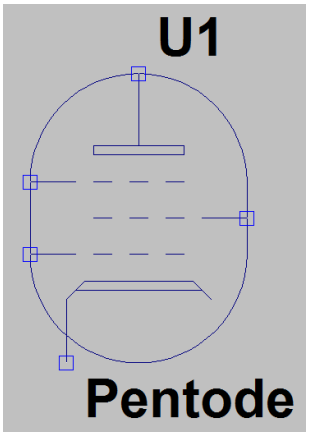

Figure 21: Left: Pentode symbol (created in LTSpice) representing the model development in Sec. 8.

Some pentodes have a separate connection for $g3$, well-known examples are the EF80 family, and, most notably, the EL34. The reason for bringing out this grid connection separately (rather than having it internally connected to the cathode) lies in the possibility of modulating on the 3rd grid.

The tube will be viewed as a pentode, consisting of the cathode, first grid, and 2nd (screen) grid; and stacked is a triode with g3 as control grid, and the anode functions as anode for both systems.

8.1 Constant space current

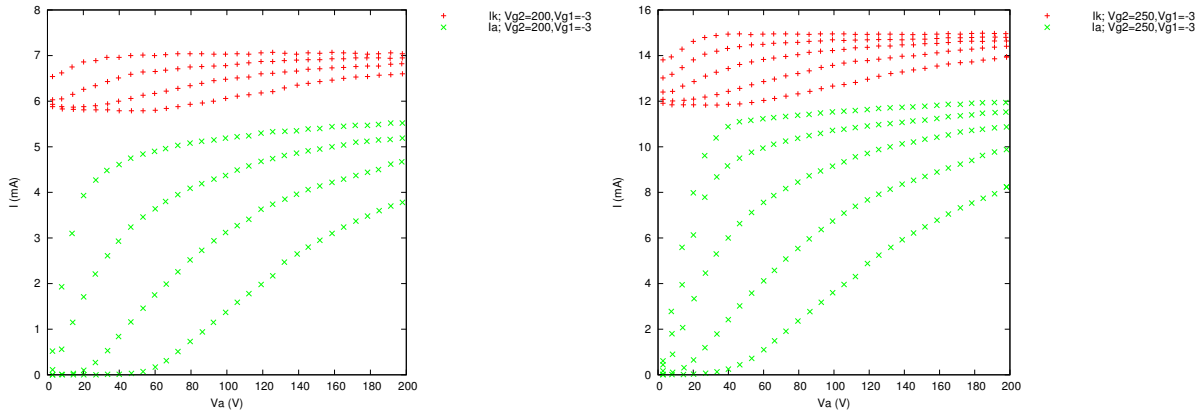

Figure 22: Space current for an EF80 at $V_{g2} = 200V$ (left) and $V_{g2} = 250V$ (right), for $V_{g1} = -3V$, and $V_{g3} = -10, -20, -30, -40V$. On the right also $V_{g3} = 0V$ is included.

The concept of constant space current proves to hold not as well for pentodes where g_3 is modulated. This is illustrated in Fig. 22 where space currents are shown for constant g_1 and g_2 voltage. The space current still shows quite some dependency on the anode voltage V_a.

That the *anode* current is dependent on V_{g3} is demonstrated by the left of Fig. 17. The anode current displays a dependency on V_a which is very similar to that of a regular triode, with the g3 as control grid. This somewhat underpins the assumption made earlier that the tube can be viewed as a pentode, and a stacked triode with g3 as control grid, and the anode functiong as anode for both

systems. An interesting observation is that with V_{g3} becoming slightly negative, the behaviour starts to resemble that of a pentode such as the EF86.

Taking a similar approach as in Secs. 4.3 and 4.4, the total space current I_c is not dependent on V_{g2}, and is written as:

$$I_c = I_a(V_a) + I_{g2}(V_a) = \frac{I_{P,1}}{k_{g_1}}(1 + AV_a - \frac{\alpha}{1+\beta V_a}) \tag{56}$$

Fig. 22 illustrates that the A parameter is has a dependence on V_{g3} - and as a general remark, the model where I_c has a linear dependence on V_a seems quite far from the truth, too. This dependence will be ignored to maintain consistency with the simple pentode model. As in the pentode case, α is not an independent parameter, see furtheron. We hence write:

$$I_{P,1}(V_{g2}, V_{g1}) = \frac{1}{2}E_{1,p}^{x}(1 + \mathrm{sgn}(E_{1,p})) \tag{57}$$

$$E_{1,p} = (\frac{V_{g2}}{k_p}) \log\left(1 + e^{k_p(1/\mu + (V_{g1}+V_{g3}/\mu_3)/\sqrt{k_{VB}+V_{g2}^2})}\right) \tag{58}$$

The space current amplification factor is given by μ_3. In subsequent references to $I_{P,1}(V_{g2}, V_{g1})$, for notational convenience the explicit dependency on V_{g2}, V_{g1} may get dropped, and reference is simply made to $I_{P,1}$.

8.2 Anode and g2 currents

We will model the pentode with g_3 as additional control grid, as a pentode, consisting of the cathode, g_1 as control grid, and g_2 as screen grid, with a triode stacked on top of that. The mazes of g_2 replace the cathode in this model, g_3 becomes the control grid. The anode serves both pentode's anode. We copy Eq. (30) describing the anode current I_a for a pentode in the `DerkE` model below:

$$I_a(V_a) = I_{\mathrm{P,Koren}}(\frac{1}{k_{g1}} - \frac{1}{k_{g2}} + \frac{AV_a}{k_{g1}} - e^{(-\beta V_a)^{3/2}}(\frac{\alpha}{k_{g1}} + \frac{\alpha_s}{k_{g2}}))$$

as the starting point.
If the triode were completely independent - one could write (see Sec. 2)

$$I_{P,2}(V_{g3}) = \frac{1}{k_{G1'}}(V_0 + V_{g3} + V_a/\mu')^{x'} \tag{59}$$

where μ' is the triode amplification factor of g_3. Note, that this behavour is a simplification of the Koren model - see Sec. 2. With the crudeness of the current model, the refinement of Koren seems inappropriate and adding only fitting parameters. In triode modelling, the parameter V_0 would be called the emission potential, and describe the effect of a charge distribution caused by the cathode and/or filament. Here, V_0 plays a similar role, although the cathode is virtual and consists of the electrons passing through g_2.

However, this model does not take into account saturation effects. The maximal current that can flow is given by the anode current Eq. (30), and therefore the triode should display saturation behaviour at that current. This is achieved by using a similar approach as in App. B.2 by re-casting Eq. (59) as:

$$I_{P,2} = 1 - e^{\frac{-1}{k_{G1'}}(V_0 + V_{g3} + V_a/\mu')^{x'}} \tag{60}$$

which displays saturation for a maximum value of $I_{P,2} = 1$, and at low values of $I_{P,2}$ is identical to Eq. (58). This transitional behaviour is not physically validated - but at least it shows the right physical behaviour at low and high V_a. Hence, the total current is

$$I_a(V_a) = I_{\mathrm{P,Koren}}(\frac{1}{k_{g1}} - \frac{1}{k_{g2}} + \frac{AV_a}{k_{g1}} - e^{(-\beta V_a)^{3/2}}(\frac{\alpha}{k_{g1}} + \frac{\alpha_s}{k_{g2}}))(1 - e^{\frac{-1}{k_{G1'}}(V_0+V_{g3}+V_a/\mu')^{x'}}) \tag{61}$$

It is evident that the anode current described by Eq. (61) for $V_{g3} = 0$ is not equivalent to Eq. (30). However, for a reasonable value of V_0, $I_{P,2}$ is substantially close to unity for $V_{g3} = 0$, and small V_a; for larger V_a $I_{P,2}$ rapidly approaches unity.

Because the anode current should equal zero at zero anode voltage, we further have as in the pentode case:

$$\frac{1}{k_{g1}} - \frac{1}{k_{g2}} = \frac{\alpha}{k_{g1}} + \frac{\alpha_s}{k_{g2}} \tag{62}$$

Hence

$$\alpha = 1 - \frac{k_{g1}}{k_{g2}}(1 + \alpha_s) \tag{63}$$

Showing that α is not an independent parameter.
From the assumption of constant space current we have

$$I_{g2} = I_c - I_a$$

describing the screen grid current I_{g2}, and concluding the full description of the tube behaviour.

In the modeling program `ExtractModel` the model described above is named 'DerkE' (see Sec. 13.1). An identical approach as outlined above can also be undertaken for the 'Derk' model. However, at this stage this model is not implemented.

8.3 Model results

In Fig. 23, the results for a screen voltage of 200V, and $V_{g1} = -3V$ are depicted.

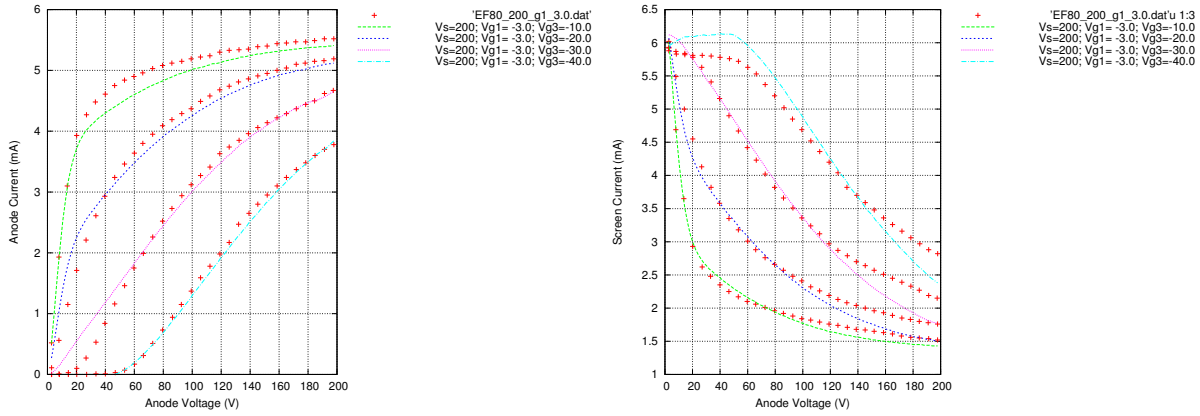

Figure 23: Anode current (left) and screen current (right) for an EF80 at $V_{g2} = 200V$, for $V_{g1} = -3V$, and $V_{g3} = -10, -20, -30, -40V$. Drawn lines are the fits according to the model of the previous section.

The model as developed in Sec. 8.2 catches the main features of the anode current dependence on V_a for various values of V_{g3}. However, the screen current is described much less well. Also evident is the

deviation of the screen current at low V_a for $V_{g3} = -40$, which is due to the fact that the space current is modelled as constant, whereas in reality the space current decreases for low V_a. As a result, the screen current is modelled too large.

While the model clearly less well captures all details compared to the previously developed models (where the assumption of constant space current proved to be excellent), the model is satisfactory for most applications. Modulating the anode current with V_{g3} is not a very linear process (and often used in class-C amplifiers, or to pinch off a tube). Hence, it is less of an issue how well the exact non-linearity is modelled.

9 Stabilizer tubes

Regulator or stabilizer tubes are a quite different breed of tubes compared to the classes of tubes discussed in prvious sections. Though these tubes were not used often in consumer equipment (radios and TVs), in professionel equipment these tubes often came to play. Particularly in oscillators, where constant anode voltages are key to maintain frequency stability, and -almost by construction - in voltage reference sources for power supplies. Also today we see some use of these tubes still in high-end valve amplifiers, where pre-amplifiers are sourced with a voltage-stabilized source to ascertain constant amplification under varying mains voltage.

9.1 Stabilizer tube model

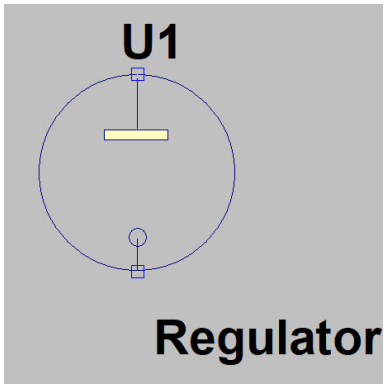

Figure 24: Regulator tube symbol (created in LTSpice) representing the model development in Sec. 9.

Stabilizer tubes typically have only two electrodes, a cathode and an anode. Also, the cathode is not heated, and the tube is filled with a gas, often a noble gas such as Neon. The tube is based on the fact that above a certain ignition voltage V_{ign}, the gas ionizes, resulting in a current through the tube from anode to cathode. The voltage required to keep the current flowing and keep the gas ionized is much lower than the ignition voltage. At the extinction voltage V_{ext} the tube will no long conduct. While the tube is conducting, current will steeply increase as a function of anode voltage, in an almost linear fashion in the region of allowed current.

This behaviour is exemplified in Fig. 25, where the current-voltage relationship for an 85A2 stabilizer tube is displayed. It is clear from this graph that - above the extinction voltage - the tube has an extremely low internal resistance (of about 300Ω). The current is almost linear in the difference $(V_{\text{a}} - V_{\text{ext}})$ above V_{ext}. This is due to the fact that the gas ionization is caused primarily by secundary electrons, that are freed up from the cathode. As in Sec. 6, the amount of secundary electrons that is freed is proportional to the energy of the incoming ions and hence the anode voltage.

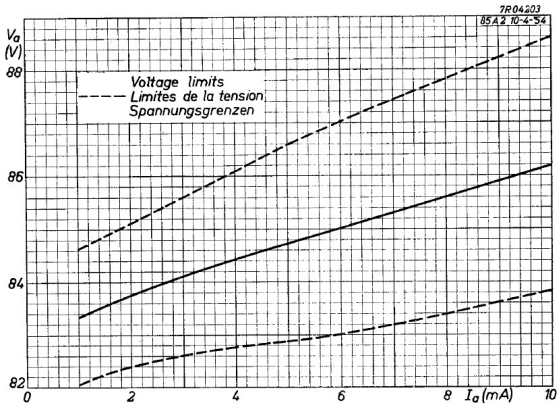

Figure 25: typical current dependence on anode voltage for the 85A2 regulator tube (Philips data sheet).

We will hence model the anode (ionization) current I_{a} as:

$$I_{\mathrm{a}} = \frac{1}{Ra} \ln(e^{a(V_{\mathrm{a}} - V_{\mathrm{ext}})} + 1) \tag{64}$$

Here a is a heuristic parameter that determines the abrubtness of the current extinction. It is important to note that this description will *only* describe the characteristics of a tube that is ignited already. The situation of increasing voltage over the tube, followed by ignition and subsequent voltage drop, is not modelled. The primary issue is that Spice simulations have no memory; *i.e.*, there is no way to determine what the trend (up or down) of the voltage is. This implies that Spice cannot deal with hysteresis in general, and, in this case, with the particular distinction of pre- or post ignition behaviour of the tube.

9.2 Models results

In Fig. 26, a Spice simulation is shown of a circuit where a supply voltage ranging from 0 to 250 V is applied to a series configuration of an 85A2 model and a 10k resistor. This nicely shows the regulating

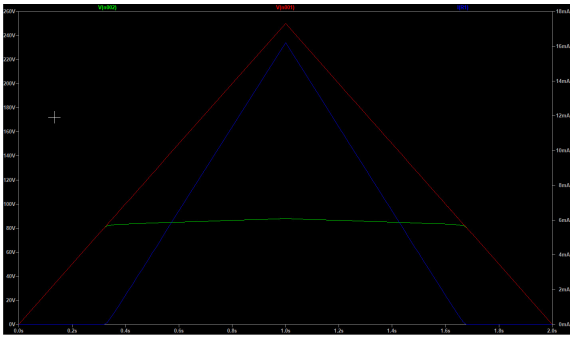

Figure 26: Spice results of the model for the 85A2 regulator tube. The regulating effect is clearly displayed as the supply voltage and reistor (and thus regulator tube) current go up from zero at $t = 0$, to a maximum of 250V for the supply voltage at $t = 1s$, back to zero again for $t = 2s$.

behaviour of the tube where initially the voltage over the tube (green curve) is rising linearly with the supply voltage, and the conducted current is zero. At reaching the extinction voltage, current starts flowing, and the voltage over the tube is kept at around 85V rather independent of the current conducted. For the down going voltage this behaviour is mirrored. As mentioned in Sec. 9.1, the behaviour of the upgoing voltage is *incorrect*, as in reality the tube will only start conducting at the ignition voltage, much higher than the extinction voltage. This behaviour, however, is impossible to model in Spice, and at least the parameter space around the operating condition of the tube is well modelled.

10 Linearized tube parameters

In circuit theory, tubes are traditionally represented in a linearized fashion [Dek43]. The most important parameters are the amplification factor A (in [Dek43] and elsewhere represented as μ; to avoid confusion with the parameter μ used in the model fitting, the symbol A is used here); the internal resistance R_i, and the steepness S of the tube. The definitions of these parameters are repeated here:

$$A = \frac{\partial V_a}{\partial V_{g1}}|_{I_a,V_a} \tag{65}$$

$$S = \frac{\partial I_a}{\partial V_{g1}}|_{I_a,V_a} \tag{66}$$

$$R_i = \frac{\partial V_a}{\partial I_a}|_{I_a,V_a} \tag{67}$$

The models derived previously allow for a precise evaluation of these parameters.

11 Fitting

11.1 Least Squares approach

In order to obtain the most accurate value of the model parameters, the model function describing the anoded and screen current will be fitted to the measured data. Measured values will be denoted by adding the subscript obs to the parameter. Without a deep underlying reason, the method of minimum least squares is chosen for this purpose. Fitting is performed for triodes by defining the function R_T^2 to be minimized as:

$$R_T^2 = \sum_{i=1,N} (I_{\mathrm{a,model},i} - I_{\mathrm{a,obs},i})^2 \tag{68}$$

And for pentodes, beam tetrodes and heptodes, the function minimized is R_P^2:

$$R_P^2 = \sum_{i=1,N} (I_{\mathrm{a,model},i} - I_{\mathrm{a,obs},i})^2 + \sum_{i=1,N} (I_{\mathrm{g2,model},i} - I_{\mathrm{g2,obs},i})^2 \tag{69}$$

Where N is the total number of data points considered in the minimization. This definition of R_P^2 implies that *e.g.* a 1mA deviation in the anode current is equally important as a 1mA deviation in the screen current. However, a 1mA deviation on a 100mA anode current is a relatively small effect, whereas a 1mA deviation on a 5mA screen current is a very significant relative deviation. From a design point of view, however, the anode currents are much more important than the screen currents, which is the reason that R_P^2 is defined to be an absolute measure of the error, rather than a relative measure. As a consequence, anode current will be fitted more accurate (in a relative sense) than screen currents.

All models have been defined such that the parameter values should be positive (to make sense physically). This means that a boundary condition in the minimization of R^2 over all model parameters p_i is that $p_i > 0$. In practice this is easy to realize by replacing the model parameters p_i by their absolute value $|p_i|$ during minimization.

11.2 Error estimates

In a perfect world, all the parameters that are fitted, are independent.If that would be true, the diagonal elements of the covariance matrix:

$$C_{ii} = (H^{-1})_{ii} \tag{70}$$

would represent the scale of the fitting errors [PTVF92].
Here **H** is the Hessian matrix:

$$H_{ij} = \frac{\partial^2 R^2}{\partial p_i \partial p_j} \tag{71}$$

The standard variance σ_i in the $i'th$ parameter p_i is subsequently given by [PTVF92]:

$$\sigma_i = \sqrt{\frac{R^2}{Nfit - 1} C_{ii}} \tag{72}$$

where $Nfit$ is the total number of parameters that is fitted. `ExtractModel` provides as output a relative error estimate $3\sigma_i/p_i$ in the parameters.

However, as shown in Sec. 3.4.1, the initial assumption of independent parameters is not correct. The error estimate that is provided, is therefore an underestimation of the real error estimate that may include correlations of other parameters.

11.3 Data fitting

For data fitting the routine 'Powell' of Numerical Recipes [PTVF92] is used. This routine is cited to be most versatile and robust, at the penalty of slow convergence close to the minimum. It has no need for function derivatives. It defines an orthogonal matrix of search directions `xi` that gets updated every iteration. After a number of iterations this matrix loses orthogonality between its columns (it loses rank) and the search becomes sub-optimal. To prevent this `xi` is re-initialized after `NFit` (the number of parameters to be optimized for) iterations to the unit matrix. Clearly this is sub-optimal, but the few seconds of CPU time that could be gained by implementing more clever methods do not outweigh the implementation effort. The order in which (at least during the first iteration) the line minimizations are carried out, is of significance. It appears that fitting those parameters that carry greatest uncertainty in their initial estimation first, is a good strategy, and is hence the implementation choice. For pentode parameter fitting, the parameters describing the Koren current are kept constant first, while only the other parameters (k_{g1},k_{g2}, A, α_s, β) (for a pentode with secondary emission ν, λ, α', w are additional) are fitted. In a second refinement, all parameters are fitted simultaneously.

11.4 Plotting

In order to have a visual assessment of the quality of the fit, the measured data is plotted with the model overlaid (see earlier figures for e.g. EL500). Because the uTracer only has a finite precision in realizing the target voltages at which the currents are measured, it often happens that a `Vs=Va` sweep is measured, where V_s can be a few volts different with respect to V_a. Likewise, in a `Vs=cst` sweep, V_s can still vary by a few volts. The model as overlaid on the data takes these variations into account; as a result, the model can look 'noisy'. This problem is remedied by locally averaging voltages, and using those instead of the actually measured voltages in the plot.

12 Initial parameter estimation

The models we want to fit the data to, are all highly non-linear, with the exception of the diode and triode models. In practice this means that the initial parameter estimate, starting the minimization, should already be rather accurate; otherwise there is a high probability that the minimization will lead to a false minimum (and there are many of those!). Hence, the key is in finding the proper starting values. In the sequel, estimates to parameters will be indicated by adding a subscript est to the parameter.

12.1 Triode model parameter estimates

12.1.1 Initial estimate μ_{est}

There are a number of limiting situations that prove to be useful to generate initial estimates for a fitting procedure; situation 1 (following) proves to be instrumental to obtaining an estimateμ_{est} of the real amplification factor μ: *Situation 1*: $V_a^2 \gg k_{VB}$; $k_p(\frac{1}{\mu} + \frac{V_g}{V_a}) \gg 1$

$$E_1 \approx \frac{V_a}{k_p} \log\left(1 + e^{k_p(1/\mu + V_g/V_a)}\right) \approx V_a(1/\mu + V_g/V_a) \tag{73}$$

And therefore:

$$I_a = \frac{(V_a/\mu + V_g)^x}{2k_{G1}}(1 + \text{sgn}(E_1)) \tag{74}$$

Which is very similar to Eq.(2) describing the model of Marshall, with the exponent of 3/2 replaced by x. In situation (1) we have the standard definition of μ and can define an estimate of $\mu_{\rm est}$ as follows:

$$\mu_{\rm est} =< \frac{V_a(V_{g,1}) - V_a(V_{g,2})}{(V_{g,1} - V_{g,2})} >_{V_{g,i}} ; I_{\rm a,obs}(V_a(V_{g,1})) = I_{\rm a,obs}(V_a(V_{g,1})) = I_\mu \tag{75}$$

Where all voltages $V_a(V_{g,i}) - V_a(V_{g,j}$ are at the same current I_μ. This basically is the definition of the amplification factor (for infinite anode impedance). Whenever no measured current $I_{\rm a,obs}(V_a(V_{g,1})) = I_\mu$ exists, an approximation is obtained by linearly extrapolation of the two neighbouring current values. We can use this equation according to situation (1) for high V_a and low $|V_g|$ only. It is a bit of a judgment call at what current level $\mu_{\rm est}$ is determined. A reasonable value for I_μ appears to be $I_\mu = 0.05 * I_{\rm max}$, where $I_{\rm max}$ is the maximum current measured. Dependent on how many different values for $V_{g,i}$ are measured, several estimates $\mu_{\rm est}$ can be generated and averaged.

12.1.2 Initial estimate for x and k_{g1}

Under identical conditions as above (situation (1), $V_a/\mu_{\rm est} > -V_g$, we write:

$$I_a \approx \frac{(\frac{V_a}{\mu} + V_g)^x}{2k_{G1}}(1 + {\rm sgn}(E_1)) \tag{76}$$

Assuming we have a reasonable estimate $\mu_{\rm est}$, this allows us to write

$$\log\left(I_{\rm a,obs}(V_a, V_g)\right) \approx -\log\left(k_{\rm g1,est}\right) + x_{\rm est}\log\left(V_a/\mu_{\rm est} + V_g\right) \tag{77}$$

Hence, plotting $\log\left(I_{\rm a,obs}\right.$ as a function of $\log\left(V_a/\mu_{\rm est} + V_g\right)$ is a straight line with intercept $\log\left(k_{\rm g1,est}\right)$ and derivative $x_{\rm est}$. Again, for a variety of values V_g this leads to a set of estimates $k_{\rm g1,est}$ and $x_{\rm est}$ that can be averaged.

12.1.3 Initial estimate $k_{\rm p,est}$ for k_p

To find an estimate for k_p, another limiting situation is convenient:

Situation 2: $V_a^2 \gg k_{VB}, k_p(1/\mu + V_g/V_a) \ll 0$

$$E_1 \approx \frac{V_p}{k_p} e^{(k_p(\frac{1}{\mu} + \frac{V_g}{V_a}))} \tag{78}$$

With I_a still given by Eq. (5). In this situation,

$$E_{1,\rm est} \approx (I_a k_{\rm G1,est})^{(1/x_{\rm est})} \tag{79}$$

and hence

$$\log E_{1,\rm est} = \log V_p - \log k_{\rm p,est} + k_{\rm p,est}(\frac{1}{\mu_{\rm est}} + \frac{V_g}{V_a}) \tag{80}$$

Hence, plotting $\log E_{1,\rm est}$ as a function of $(\frac{1}{\mu_{\rm est}} + \frac{V_g}{V_a})$, this is a straight line with derivative $k_{\rm p,est}$; we ignore the small dependency on $k_{\rm p,est}$ of the intercept.

12.1.4 Initial estimate for k_{VB}

Situation 3: $k_p(\frac{1}{\mu} + \frac{V_G}{V_a}) \gg 1$ In this case we can write Eq. (4) as

$$E_1 \approx V_a(\frac{1}{\mu} + \frac{V_G}{\sqrt{(k_{VB} + V_a^2)}}) \tag{81}$$

With I_a still given by Eq. (5). This equation can simply be solved for k_{VB} using $\mu = \mu_{\rm est}$, and multiple obtained values for different V_a and V_g can be averaged.

12.2 Pentode model parameter estimates

The initial parameter estimates $\mu_{\rm est}, x_{\rm est}, k_{\rm p,est}, k_{\rm g1,est}, k_{\rm VB,est}$ in any of the pentode models can most conveniently be obtained by first strapping the pentode as a triode, and fitting the Koren triode model to the observed data. This leaves as a next step to still obtain initial parameter estimates for the parameters that are specific to the pentode models.

12.2.1 Initial estimate for $k_{g2,\rm est}$

We obtain an estimate for k_{g2} by looking at the screen current for high anode voltages:

$$I_{g2}(V_a \gg 1) \approx \frac{I_{\rm P,Koren}(V_{g1}, V_{g2}}{k_{g2}}) \tag{82}$$

And the estimate $k_{g2,\rm est}$ is obtained as

$$k_{g2,\rm est} =< \frac{I_{\rm P,koren,est}(V_{g1}, V_{g2})}{I_{g2,\rm obs}}) >_{V_{g1},V_{g2}} \tag{83}$$

Where we use the symbol $I_{\rm P,koren,est}(V_{g1}, V_{g2})$ as a short-hand notation for the Koren current as defined by all parameter estimates:$I_{\rm P,Koren}(V_{g1}, V_{g2}; \mu_{\rm est}, x_{\rm est}, ...)$.

12.2.2 Initial estimate $A_{\rm est}$

For high V_a we see that the anode current has a slope that is determined only by A/k_{g1}:

$$\frac{\partial I_a(V_a \gg 1)}{\partial V_a}) = I_{\rm P,Koren}\frac{A}{k_{g1}} \tag{84}$$

Hence we obtain the estimate

$$(\frac{A}{k_{g1}})_{\rm est} =< \frac{1}{I_{\rm P,Koren,est}(V_{g1}, V_{g2})}\frac{\partial I_{a,\rm obs}(V_a)}{\partial V_a} >_{(V_{g1},V_{g2})} \tag{85}$$

And

$$A_{\rm est} = k_{g1,\rm est}(\frac{A}{k_{g1}})_{\rm est} \tag{86}$$

12.2.3 Initial estimate $\alpha_{s,\rm est}$ and $\beta_{\rm est}$ (Derk model)

For very small V_a, the screen current can be approximated as:

$$I_{g2}(V_a \approx 1) \approx \frac{I_{\rm P,Koren}}{k_{g2}}(1 + \frac{\alpha_s}{1 + \beta V_a}) \tag{87}$$

Hence, if we plot $(\frac{k_{g2,\rm est} I_{g2,\rm obs}(V_a)}{I_{\rm P,Koren,est}} - 1)^{-1}$ as a function of V_a, this should be a straight line with intercept b and derivative a. Executing a fit of a straight line for all V_{g1} and V_{g2} and averaging this over all V_{g1} and V_{g2} to obtain $< a >_{(V_{g1},V_{g2})}$ and $< b >_{(V_{g1},V_{g2})}$ we get

$$\alpha_{s,\rm est} = \frac{1}{< b >_{(V_{g1},V_{g2})}}$$

$$\beta_{\rm est} = \alpha_{s,\rm est} < a >_{(V_{g1},V_{g2})} \tag{88}$$

12.2.4 Initial estimate $\alpha_{s,\text{est}}$ and β_{est} (DerkE pentode model)

For very small V_a, the screen current can be approximated as:

$$I_{g2}(V_a \approx 1) \approx \frac{I_{\text{P,Koren}}}{k_{g2}}(1 + \alpha_s e^{-(\beta V_a)^{(3/2)}}) \tag{89}$$

Hence, if we plot $\log(\frac{k_{g2,\text{est}} I_{g2,\text{obs}}(V_a)}{I_{\text{P,Koren,est}}} - 1)$ as a function of $V_a^{(3/2)}$, this should be a straight line with intercept b and derivative a. Executing a fit of a straight line for all V_{g1} and V_{g2} and averaging this over all V_{g1} and V_{g2} to obtain $< a >_{(V_{g1},V_{g2})}$ and $< b >_{(V_{g1},V_{g2})}$ we get

$$\alpha_{s,\text{est}} = e^{<b>_{(V_{g1},V_{g2})}}$$

$$\beta_{\text{est}} = (< -a >_{(V_{g1},V_{g2})})^{(2/3)} \tag{90}$$

12.3 Variable-mu pentode model parameter estimates

As for regular pentode as described in Sec. **??**, the initial parameter estimates $\mu_{\text{est}}, x_{\text{est}}, k_{\text{p,est}}, k_{\text{g1,est}}, k_{\text{VB,est}}$ in any of the pentode models is most conveniently be obtained by first strapping the pentode as a triode, and fitting the Koren triode model to the observed data. However, as already mentioned in Sec. 5, this may produce results that are not realistic nor trustworthy. In particular it may be required that the maximum cathode current `Icmax` for which data are fitted, is severely limited. For most variable-mu pentodes, the region of cross-over is around 0.5-2 mA. For a triode fit this would imply that limiting `Icmax` to about 1mA provides a fit of the low-mu region of the pentode. In practice this has shown to give excellent results; however the overall fit will look very bad (as the high mu part is not fitted at all!). The success of this approach can be checked by evaluating the fitted value of μ - this value should be typically less than 100. A value larger than than that typically indicates that an incorrect optimum has been found.
While the aboves give the initial values for the set of μ_a, x_a, another set of μ_b, x_b is estimated by changing the initially found values by 50% and 20%, respectively. The parameter s_{var} is set to 0.5 which as $0 \leq s_{\text{var}} \leq 1$ seems a reasonable value.

This leaves as a next step to still obtain initial parameter estimates for the parameters that are specific to the pentode models.

Subsequently all other parameters are estimated as described in Sec. **??**, while replacing $I_{\text{P,Koren}}$ by $I_{\text{P,Koren}_v}$.

12.4 Secondary emission model parameter estimates

The estimation for the parameters α_s and β follows in an identical manner as for the 2nd pentode model. This estimate however may suffer from inaccuracies due to the effects of the secondary emission; the estimate for α_s and β is done at low anode voltages, which is exactly where secondary emission is relevant.

12.4.1 Initial estimate $\lambda_{\text{est}}, \nu_{\text{est}}$ and w_{est}

The estimation of λ_{est} is based on the assumption that $\lambda_{\text{est}} \approx \mu$, and hence we set $\lambda_{\text{est}} = \mu_{\text{est}}$. ν_{est} and w_{est} is based on determining the local maximum if it exists, or the local inflection point, that occurs in the screen current $I_{g2}(V_a, V_{g2}, V_{g1})$ at an anode voltage $V_{a,\max}$; denote this by

$$I_{g2,\max}(V_{g2}, V_{g1}) = I_{g2}(V_{a,\max}, V_{g2}, V_{g1}) \tag{91}$$

If no maximum, and no inflection point can be detected, $V_{a,\max}$ is set to zero. Hence we can set

$$V_{a,\max} - V_{g2}/\lambda_{\text{est}} = -\nu_{\text{est}} V_{g1} - w_{\text{est}} \tag{92}$$

and plot $V_{a,\max}$ as a function of V_{g1}. This should be a straight line with derivative $-\nu_{\text{est}}$ and intercept w_{est}. If in no measured curve maxima or inflection points can be detected, the initial parameter values ν_{est} and w_{est} are set to zero, and a message is issued that it might be worthwhile to try a fit without secondary emission effects instead. During the fitting procedure, all secondary emission parameters will still be optimized; however often the results are non-physical and only lead to aesthetical improvements of the fit.

12.4.2 Initial estimate S_{est}

To obtain the estimate S_{est}, we estimate the contribution P_{sec} of the secondary emission to the screen current $I_{g2,\max}(V_{g2}, V_{g1})$:

$$\frac{I_{\text{P,Koren,est}}}{k_{g2}} P_{\text{sec,est}}(V_{g1}, V_{g2}) = I_{g2,\max}(V_{g2}, V_{g1}) - \frac{I_{\text{P,Koren,est}}(V_{g2}, V_{g1})}{k_{g2}} (1 + \alpha_s e^{-(\beta_{\text{est}} V_{a,\max})^{(3/2)}}) \tag{93}$$

And thus, taking the average over all values (V_{g1}, V_{g2}), we obtain:

$$S_{\text{est}} = < \frac{k_{g2} P_{\text{sec,est}}(V_{g1}, V_{g2})}{2 V_{a,\max} I_{\text{P,Koren,est}}} >_{(V_{g1}, V_{g2})} \tag{94}$$

12.4.3 Initial estimate $a_{p,\text{est}}$

We simply set $a_{p,\text{est}} = 0.2$. This proves to be a reasonable value that is close to the results of fitting the secondary emission model to many power tubes. There is no physical rationale to this value.

12.5 Heptode parameter estimation

The heptode model contains the standard set of parameters of the Koren current $I_{\text{P,Koren}}$; the initial parameter estimates $\mu_{\text{est}}, x_{\text{est}}, k_{\text{p,est}}, k_{\text{g1,est}}, k_{\text{VB,est}}$ can most conveniently be obtained by first strapping the heptode as a triode, and fitting the Koren triode model to the sum $I_a + I_{g2g4}$ of the observed data. These initial estimates to these are obtained by fitting a dataset of a 'Vs=Va' sweep with constant V_{g3} - or if desired a set of files with multiple different values of V_{g3}. This leaves as a next step to still obtain initial parameter estimates for the parameters that are specific to the heptode models. The first parameter that needs estimation is μ_3. Experience has shown that for most tubes, $\mu_3 \ll 10$. A reasonable starting parameter therefore is $\mu_3 = 100$. Variations by a factor of two of this value have not shown any impact on final refinement values in the (limited) experience so far. For the estimate of α and β the procedure as outlined in Sec. 12.2.3 is followed.

This leaves the initial estimation of the parameters $\mu'_{\text{est}}, x'_{\text{est}}, k'_{\text{p,est}}, k'_{\text{VB,est}}$ in $I_{H,2}$ (see Eq. (51)). These parameters can be easiest obtained by a fit to the Koren triode model of the anode current of a heptode, strapped as triode, for constant V_{g1} and various V_{g3} values. This leaves as only further parameter $k'_{\text{g1,est}}$, which estimate is obtained based on the fact that

$$I_{H,2}/k'_{\text{g1}} < p < 1$$

In `ExtractModel`, p is - rather arbitrarily - set to 0.1.

13 The program ExtractModel

A program called ExtractModel has been written to fit the models discussed in the previous sections to a dataset obtained by the uTracer of Ronald Dekker. The uTracer can generate a file with extension `.utd` that contains a table of all measured values, which serves as input to `ExtractModel`. The uTracer can perform different kinds of parameter sweeps. For diodes there are multiple sweeps that can be used; the primary requirement is that I_a is measured as function of V_a. To remain consistent with sweeps used for other tubes it is advised to stick to the 'I(Va,Vg) with Vs, Vh constant' sweep. It is sufficient to enter only one V_g value (the value of which is irrelevant as V_g is not used; as long as $V_g < 0$ to meet the `uTracer` requirements).

For triodes, the sweep that is used by `ExtractModel` is the 'I(Va,Vg) with Vs, Vh constant' or `Vs=cst` sweep for triodes or penthodes. This sweep performs a measurement of the anode current as a function of anode voltage, and does so for various grid voltages V_{g1}. While this sweep is sufficient to fit all parameters for a triode model, for a penthode model different values of V_s are required, too. This is done by repeating the 'I(Va,Vg) with Vs, Vh constant' sweep for various screen voltages V_s, and storing the data files separately. In addition the 'I(Va=Vs,Vg) with Vh constant' or `Vs=Va` sweep is used for penthodes to generate the triode model of the penthode, to generate the initial parameter values (see Sec. 12.2). The program is written in fortran; microsoft fortran is used for compilation under Windows, and gfortran for compilation under Linux. The user interface is simple text based, aiding in easy portability over different platforms. No attempt is made for any algorithmic optimization for speed as focus has been on both robustness and ease of model development.

13.1 Initialization file description

An initialization file (by default 'Model.ini'; different names can be used as command line arguments) is required to provide all necessary inputs to `ExtractModel`:

```
C:\Program Files (x86)\gnuplot\bin\wgnuplot.exe !location of gnuplot executable
3 !number of .utd files
data1 !as many .utd files as the number above indicates
data2 !as many .utd files as the number above indicates
data3 !as many .utd files as the number above indicates
P !D(Diode),T(Triode), X(Penthode/triode mode), P(Penthode), B(beam tetrode), H(Heptode), F(Pe
Derk !Model used; either Koren, Derk or DerkE
2. !Pmax in fit !fitting only data points below P=Pmax curve
0 !Vg Offset !Offset to grid voltage
```

Optional is an entry

```
Icmax = xxx
RdStart = <StartParfilename>
```

where `xxx` is the maximum cathode current in the data file that is used for fitting. If this entry is left out, there is no limit to the cathode current used. `StartParfilename` is the name of a file that contains initial parameter estimates that will be used - rather than the values that would be generated automatically by `ExtractModel`. The format of the file should be identical to the format that the `.par` output files have.
Following is a line-by-line description of the input required in the initialization file:

1. `ExtractModel`uses gnuplot [Gnu13] as the utility to create plots of the data and the curves that have been fitted to the data. Hence, ExtractModel needs to know where the executable of `Gnuplot` is located.

2. The number of `.utd` datafiles, see Sec. 13.2 for input filename conventions. For penthodes and beam tetrodes, multiple files with sweeps using different values for Vs are required. The maximum number of files is set to 15. For triodes the number of files can be larger than 1 if multiple tubes have been measured, and the fit needs to represent an average of the different tubes. As tubes can differ easily by 10% in current for identical voltages, this is a nice way to get a representation of the 'average tube'.

3. The names of the data files. The extension `.utd` must be left out. If fitting a penthode / beam tetrode, the last file can be the file as measured in 'triode mode', i.e. in a `Vs=Va` sweep. If a `Vs=Va` data file is listed, but *not* as the last file, this will stop `ExtractModel`.

4. The type of tube. Currently the choice of tubes is

   (a) D - for a diode

   (b) T - for a triode

   (c) X - for a penthode, but measured with the 'I(Va=Vs, Vg) with Vh constant' sweep. This signals `ExtractModel`to sum the anode and screen currents, and fit a triode model

   (d) Y - for a hepthode, measured with the 'I(Va=Vs, Vg) with Vh constant' sweep (and for a specific Vg3). The use of this tube designator signals `ExtractModel` to create a parameter file `Triode_g3.par` that is used as input for starting parameters in the heptode model fitting (see Sec. 12.5)

   (e) P - for a penthode. For historical (programming) reasons, this tube designation is used if secundary emission is not playing any role. It can be used with both the Derk and DerkE models.

   (f) V - for a variable-mu penthode. For historical (programming) reasons, this tube designation is used if secundary emission is not playing any role. It can be used with both the Derk and DerkE models.

   (g) B - for a beam tetrode. For historical (programming) reasons, this is the tube designation that includes secundary emission effects. It can be used with both the Derk and DerkE models.

   (h) H - for a Hepthode.

   (i) F - for a penthode with g3 modulation

5. Model used for fitting. Known model names are 'Koren', 'Derk' (see Sec. 4.4) ('DerkI' is also possible - see App. **??**) and 'DerkE' (see Sec. 4.5). For diodes and triodes, the only available model is 'Koren'; whenever a different name is given, it is still fitted according to the Koren model. For hepthodes, the only available model is 'Derk'.

6. The maximum anode dissipation Pmax used in fitting the data; only data for which $I_a V_a < P_{\max}$ is used to fit the data to.

7. The uTracer can only generate grid voltages between -49 and 0 volts. VgOffset is any constant voltage that is added to that by an external source to create grid voltages below -49V.

13.2 Input file naming

The input filename conventions are not very strict for diodes and triodes, except for the fact that the filename extension should be `.utd`. A choice the author makes is to just call the file to the tube naming, *e.g.*, `ECC81.utd` or `PCF80C.utd`. For penthodes, more files are needed. Again, there are no strict rules to naming. A choice the author makes is to have a naming that indicates whether the tube has been measured in triode mode or with a fixed V_{g2} bias, *e.g.* `PF86_triode.utd`, which would be a PF86 measured in triode mode, and `PF86_200.utd` which would be a PF86 measured at $V_{g2} = 200V$. In all cases, the exact parameter values will be read from the data file itself.

For heptodes the naming is no longer free. Heptode data files need to be generated with both V_{g1} as a variable, and with V_{g3} as a variable, and the uTracer does not allow storing these as separate variables. The trick that needs to be played is to run several 'I(Va=Vs, Vg) with Vh constant' sweeps, where either V_{g1} or V_{g3} is connected to the V_g terminal. Naming the datafile has therefore has to be according to the following convention:

filename = `abcdefgh_gn_xx.x.utd`

where n denotes the grid (either 1 or 3); and xx.x denotes the constant voltage that has been applied to that grid during the scan. An example is `ECH81_100_g3_10.0.utd`. This is a dataset where V_{g2} is kept at a constant voltage of 100V ('I(Va, Vg) with Vs, Vh constant' sweep), which will be reflected in the data it self. The first grid $g1$ is connected to the V_g terminal, and V_{g3} has been kept constant by an external voltage source to $-10.0V$. This voltage is not represented in the dataset, and the only way for `ExtractModel` to know this voltage is the filename. Another example is `ECH81_triode_g1_1.5.utd`. This represents a 'I(Va=Vs, Vg) with Vh constant' sweep, where an external source has been used to set $V_{g1} = -1.5V$. This implies that $g3$ of the heptode has been connected to the V_g terminal of the uTracer, and, hence, that the data tabulated in the file, has a variable V_{g3}.

13.3 Output files

The most important outputfile is 'data1.cir', which is a concatenation of the first data file name in the initialization file, and the '.cir' extension. This is the LTSpice file containing the model of the tube that has been fitted.

```
*****************************************************
 .SUBCKT ECC85 1 2 3; A G C;
* ExtractModel V .995
* Model created: 29-Nov-13
X1 1 2 3 TriodeK MU= 94.0 EX=1.148 kG1=  59.9 KP= 230.9 KVB=3805. RGI=2000
+ CCG=0.0P  CGP=0.0P CCP=0.0P  ;
.ENDS

*****************************************************
.SUBCKT TriodeK 1 2 3; A G C
E1 7 0 VALUE=
+{V(1,3)/KP*LOG(1+EXP(KP*(1/MU+V(2,3)/SQRT(KVB+V(1,3)*V(1,3)))))}
RE1 7 0 1G
G1 1 3 VALUE={0.5*(PWR(V(7),EX)+PWRS(V(7),EX))/kG1}
RCP 1 3 1G    ; TO AVOID FLOATING NODES IN MU-FOLLOWER
C1 2 3 {CCG}  ; CATHODE-GRID
C2 2 1 {CGP}  ; GRID-PLATE
C3 1 3 {CCP}  ; CATHODE-PLATE
```

```
D3 5 3 DX     ; FOR GRID CURRENT
R1 2 5 {RGI}  ; FOR GRID CURRENT
.MODEL DX D(IS=1N RS=1 CJO=10PF TT=1N)
.ENDS TriodeK
```

The `.cir` file contains the Spice definition of the model, DiodeK, TriodeK, PenthodeD, PentodeDE, PenthodeB, PenthodeBE, or HeptodeD, and the tube specific description of the parameterset feeding the model. Also note that the signum function (see Eq. (5)) is implemented consistenly for all models. When a library of tubemodels is made, the Spice definitions of the models need to be copied only once, thereafter only the tube specific parameter description needs to be copied. The Spice code generated for a Triode is based on the code as proposed by Koren ([Kor01]). The code contains parametric descriptions of the inter-electrode capacitances, that are all set to zero in the output of ExtractModel. The user will have to add these based on datasheet reported values. Other files that are created are a `Model.par` file, which contains the refined parameters, and, if a triode type 'X' was fitted, a `Triode.par` file which can be used as input for fitting a penthode model later. Further output files are the files that are fed to `Gnuplot` to do the plotting. The plot file for display of the anode currents is the `.plt` file; the plot file with extension `.spl` loads and displays the screen currents. Note that this extension is also used by Shockwave. These files can be loaded in Gnuplot any time later to review the fitting results, independent of `ExtractModel`.

13.4 Model fitting tips

Feedback from users working with `ExtractModel` has generated some practical tips for a good fit, and listed in the following. `ExtractModel`already incorporates, or will incorporate, some of the tips below and generate warnings when the data to be fitted is insufficient (sec. 13.4.1), when the tube displays saturation effects (sec. 13.4.2), or when the dynamic range is too large for a good fit (sec. 13.4.3). `ExtractModel` will leave it to the discretion of the user to continue - but results may not be correct.

13.4.1 Number of different values for V_g

For a triode fit, different values for V_g are required to get a good estimate of especially the parameter k_p. Depending on how accurate the measurements are, at least 5 different values for V_g are required, and at least a few values are needed that give an accurate description of the cut-off behaviour, which helps in good estimates of k_{VB}. This means that several V_g values should be present that have a region where the anode current is zero within the precision of the uTracer. Preferably (see also Sec. 13.4.3 one would have a range of V_g values which, at the maximum anode voltage and highest V_g, result in an anode current of about 150% of the maximum anode current, and at the maximum anode voltage and lowest V_g about 20% of that. Fig. 1 gives an idea for two different triodes. For regular penthodes, at least 3 different values of V_{g2} are required, and per V_{g2} value at least 3 different values for V_g. Variable-mu pentodes - on the contrary - require a large number of different values for v_{g1}, preferably evenly spread over the high-mu and low-mu characteristic of the pentode.

13.4.2 Saturation

Saturation of a tube is a phenomenon where the cathode is not capable of delivering the current that theoretically would flow, see also [Spa48] for a description of this phenomenon. For triodes, the anode current as function of anode voltage show a positive curvature (the curve becomes ever steeper with increasing anode voltage). Severe saturation will cause the anode current to show negative curvature (*i.e.*, the steepness of current increase as a function of voltage becomes less). It is important to remove

curves that display this behaviour while fitting. `ExtractModel` will try to fit the measurements (even though in very severe cases, it gives a warning); and as a result the fitted parameter values may not represent the true behaviour.

For penthodes, saturation may occur either due to excessive screen current at low anode voltage, or, similar as with a triode, due to excessive anode current at very high anode voltages. Saturation at low anode voltages can be detected by inspection of the screen current, which, at low anode voltages, should be a concave curve. When this curve becomes convex, saturation plays a role. Especially when secundary emission is included in the model fitting, `ExtractModel` may easily be fooled by the convex part in the screen current, and mistakenly interprets it as secundary emission (which also causes convex curvature of the screen current!).

As a rule of thumb, one should never have data with cathode currents that largely exceed the maximum values as published in the datasheets. For new tubes of reknowned brands, the cathode can typically deliver 150% of the tabulated maximum value. This is often not true for some russian NOS stubes, and old, used tubes that already spent a good deal of their life in heavy duty.

13.4.3 Dynamic range

The previous section Sec. 13.4.2 already implicitly gave an upper boundary for the current measurements. Curves reaching lower current values are required for covering the full space that is needed for a good parameter fit - however, if currents are very close to zero over the full anode voltage range, this adds no information (and actually detracts `ExtractModel`). Typically, a good dynamic range is between 5 and 10, meaning that the highest current reached for the V_g, V_{g2} combination that gives the lowest overall current, should be no less than about 1/10 to 1/5 of the maximum current over all parameters. Good examples for this are the curves presented throughout this document, where the dynamic range never exceeds 7.

For vaiable-mu pentodes, care should be taken that all curves cover the high-mu and low-mu part of the characteristic evenly. A dataset with many values for the low-mu part, and few for the high-mu part will give an untrustworthy result. Note that this is a mistake easily made, since an evenly distributed set of grid values V_{g1} will likely correspond to a few high-mu values, and many more low-mu values.

13.4.4 Data range

In particular with heptodes, it is important to play a bit with the maximum anode dissipation and/or maximum cathode current of the data used for fitting. The heptode model can easily get caught in a false minimum if the maximum power/current used in fitting is too large. This leads to the interesting effect that the fit can sometimes (even for high currents) be better if the data used in the fit is restricted to values of 0.5W or even a bit below for the anode dissipation. Until initial parameter estimation is improved, this inconvenience has to be accepted.

14 Spice implementations

The program creates a spice model in the LTSpice dialect. LT Spice is available in the public domain through the web site of Linear Technology [Lin13].

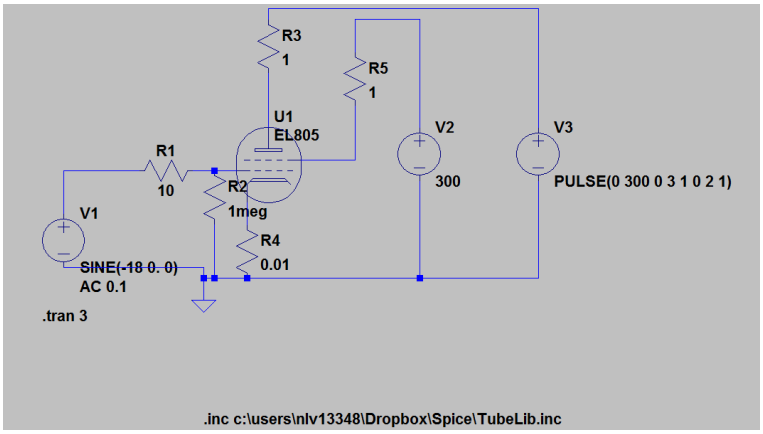

Figure 27: Spice test circuit for the models generated by `ExtractModel`.

In Fig. 27, the test circuit is depicted to generate the test curves of the spice models. The anode voltage is a ramp from 0 to 300V over 3s; in a transient simulation this equates to 100 V per second.

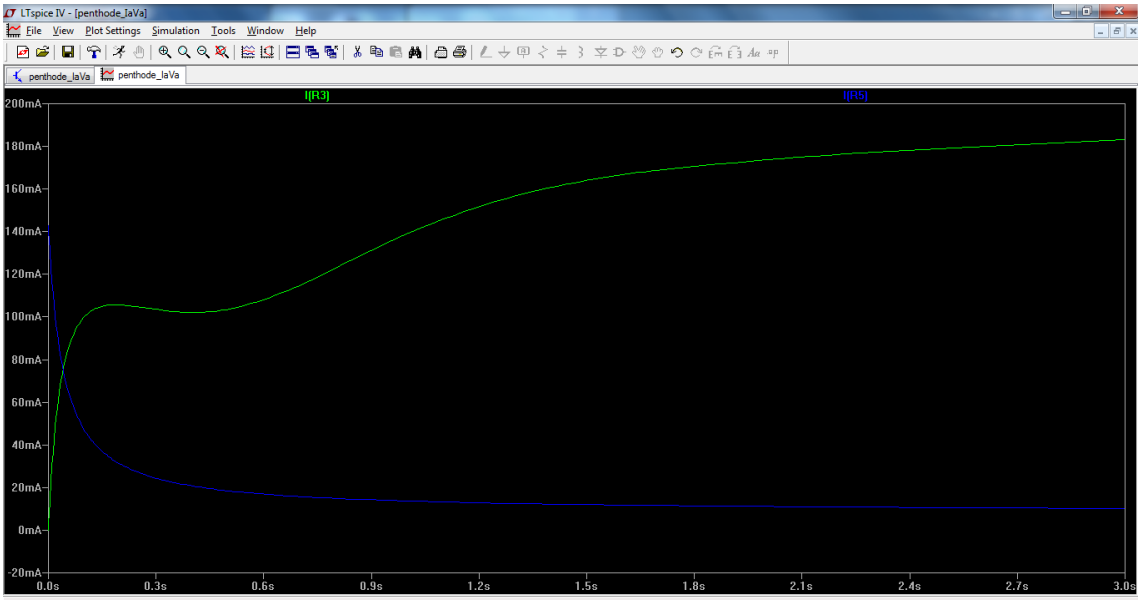

Figure 28: Simulation result of the Spice test circuit of Fig. 27.

A typical result is depicted in Fig. 28 for the EL805, showing anode and screen currents, corresponding to the curve shown for the EL805 in Fig. 29.

15 Acknowledgements

A lot of people have given constructive feedback leading to continuous improvement of the model development, and of the ExtractModel program. In particular I want to thank Rogelio Baucells for the interesting discussions on model stability, which has led to the insights discussed in Sec. 3.4.1. I want to thank Nick Barton for his critical reading of the document, and providing suggestions for improvements.

Appendices

A Constant Space Current

Constant space charge - and therefore a cathode current I_k independent of the anode voltage V_a - is the key assumption for the derivation of the new pentode models. While this assumption is made widely in much of the literature (see *e.g.* [Spa48]) this appendix serves as a re-assurance of the validity of this assumption.

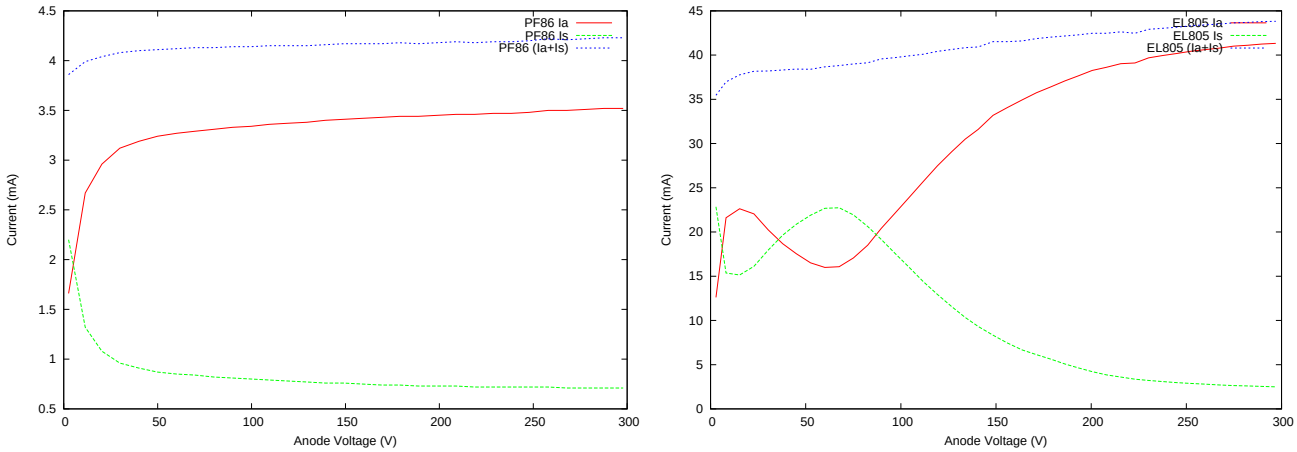

Figure 29: Demonstration of constant space charge for the EL805.

In Fig. 29, typical anode, screen and cathode current for an almost ideal small signal pentode PF86 and a power pentode EL805 are depicted. Clearly, the power pentode displays significant effects due to secondary emission, which are absent in the curves for the PF86. Still, the sum of the anode and screen current (i.e. the cathode current) is almost constant for both cases, illustrating and validating the concept of constant space charge / current.

B pentode scaling behaviour

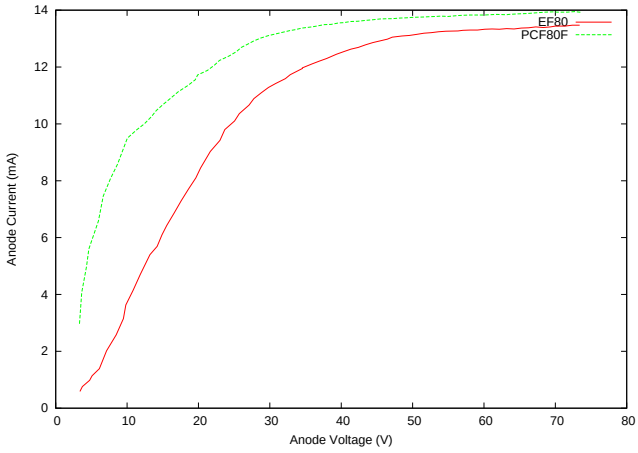

Figure 30: Low anode voltage behaviour of the anode current for an EF80 and PCF80(F).

In Fig 30, the low anode voltage behaviour of a real pentode (the F-section of a PCF80) and that of a a pentode exhibiting pentode beam behaviour is depicted. Clearly the two behaviours are distinctly different. The PCF80F shows a convex increase in anode current at low voltages already, whereas the EF80 displays a concave behaviour. It is therefore necessary to separate the two cases in modelling the characteristics.

B.1 Real pentode scaling behaviour

Much work has been devoted in the early years of vacuum tube technology to understand the ratio of anode and grid current for triodes. The reason for this is that, when a triode is operated at positive grid voltage, it starts to behave much like a current source (similar to a pentode): its $I_a - V_a$ characteristic becomes more and more flat. This is important for power triodes, as the power efficiency substantially increases as the triode is more acting as a current source. From this early work, it becomes apparent that within certain approximations, the ratio of anode and grid currents is given by:

$$\frac{I_a}{I_g} = \frac{LV_g + MV_a}{PV_g + QV_a} \tag{95}$$

which is Eq. 9.28b in [Spa48]. The parameters L, M, P and Q are given by the tube geometry. The reader should consult [Spa48] for the details. For a pentode, it is the grid $g2$ that is at positive potential. We will copy the analysis for a triode tube operated with positive grid, for the screen grid of a pentode.

On the assumption of constant space current in a pentode, we can write:

$$I_k = I_{g2}(\frac{L + M\frac{V_a}{V_{g2}}}{P + Q\frac{V_a}{V_{g2}}} + 1)$$

where I_k is the cathode current - and proportional to the Koren current $I_{\mathrm{P,Koren}}$ used throughout the document. Hence we can write:

$$I_{g2} \propto I_{\mathrm{P,Koren}} \frac{P + Q\frac{V_a}{V_{g2}}}{L + P + (M + Q)\frac{V_a}{V_{g2}}}$$

For screen grid voltages V_{g2} which are close to the anode voltage V_a, $P \ll Q\frac{V_a}{V_{g2}}$. Note, that for triodes this may not true, as the grid will typically be run at voltages only a tiny fraction of the anode voltage! Hence, keeping the number of fitting parameters minimal, for pentodes a good scaling behaviour is given by:

$$I_{g2} \propto I_{\mathrm{P,Koren}}(1 + \frac{\alpha_s}{1 + \beta' \frac{V_a}{V_{g2}}}) \tag{96}$$

Arguably, for screen voltages that do not vary too much (in practical circumstances, the screen voltage is never varied by much more than 50%), this can further be simplified to

$$I_{g2} \propto I_{\mathrm{P,Koren}}(1 + \frac{\alpha_s}{1 + \beta V_a})$$

leading to Eq. (23):

$$I_{g2}(V_a) = \frac{I_{\mathrm{P,Koren}}}{k_{g2}}(1 + \frac{\alpha_s}{(1 + \beta V_a)})$$

which is the default pentode model used by `ExtractModel`, and named 'Derk'. Practice has shown fit results based on Eq. (96) and Eq. (23) to differ marginally, χ^2 values differing by about 1%, sometimes in favour of Eq. (96), and sometimes in favour of Eq. (23). The model that represents Eq. (96) (the *Original* model) is also available in `ExtractModel` by setting `model` to `DerkI`.

B.2 Beam tetrode scaling behaviour

A detailed analysis of beam tetrode behaviour has been performed by O. H. Schade [Sch38]. Due to the space charge, a virtual cathode is created in the space between the screen grid and the anode: this is the position at which the electron velocity has decelerated to practically zero. This virtual cathode only exists for relatively low anode voltages. Interestingly, the virtual cathode sees only the anode; and hence the virtual cathode and the anode form a virtual diode that is in series with the real cathode and the control and screen grid. At low anode voltages this diode displays a behaviour which is behaves as a regular diode, i.e. its current is roughly proportional to $V_a^{(3/2)}$ (see Sec. 2). At a certain anode voltage, the virtual cathode ceases to exist: there is no point in space between the screen and anode where the potential is zero, and all electrons pass: the virtual diode is saturated, causing the familiar kink in the beam tetrode curve (the 'knee'). The way this behaviour is described in `ExtractModel` is with

$$I_a \propto 1 - e^{-(\beta V_a)^{(3/2)}} \tag{97}$$

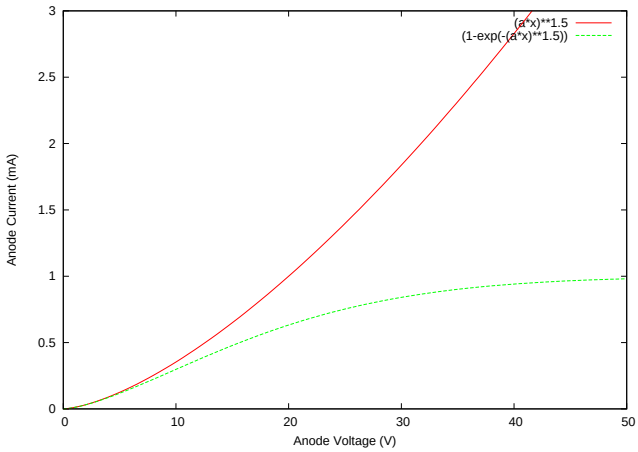

Figure 31: Modelling the low anode voltage behaviour of the virtual diode. In red, the power (3/2) behaviour; in green the behaviour including saturation ('kink').

As demonstrated in Fig. 31, for low anode voltages, this scaling behaviour describes the virtual diode behaviour with the Langmuir current behavior

$$I_a \propto (\beta V_a)^{(3/2)}$$

At higher voltages saturation is reached, described by the exponential behaviour. The exact function describing the saturation is very complex and depends on many parameters, like the alignment of the grids, the exact distances of the grids to the anode etc. No effort has been made to describe this transition accurately. The graph displays the behaviour of the scaling function, and how it displays the Langmuir dependency of current on voltage.

References

[Adr14] Andre Adrian. History of the vacuum tube theory, spice models. http://www.andreadrian.de/roehrenverstaerker/hvtt_20140331.pdf, 2014.

[Dek43] J. Deketh. *Grondslagen van de radiobuizentechniek*. N.V. Philips' Gloeilampenfabrieken te Eindhoven, 1943.

[Dek13] Ronald Dekker. The utracer, a miniature tube tester/curve tracer. www.dos4ever.com/uTracer3/uTracer3.html, 2013.

[Exc95] Excem vacuum tube modeling package vol. 1 1995. http://www.excem.fr/download/usergui5.pdf, 1995.

[Gnu13] www.gnuplot.info, 2013. Release used in preparing this document is: 09.10.2013: Release gnuplot 4.6.4.

[Kor96] Norman Koren. Improved vacuum tube models for spice simulations. *Glass Audio*, 8, 1996.

[Kor01] Norman Koren. http://www.normankoren.com/Audio/Tubemodspice_article.html, 2001.

[Lin13] Ltspice. www.linear.com/designtools/software/, 2013.

[MB14] Suusi Malcolm-Brown. Tube library 20 april 2014. http://www.mif.pg.gda.pl/homepages/frank/other/docs/Koren_Tubes.cir, 2014.

[Per98] Stefano Perugini. Vacuum diode models and pspice simulations. *Glass Audio*, 10, 1998.

[PTVF92] William Press, Saul Teukolsky, William Vetterling, and Brian Flannery. *Numerical Recipes in Fortran 77*. Second edition edition, 1992.

[Rey93] Scott Reynolds. Vacuum-tube models for pspice simulations. *Glass Audio*, 5:17, 1993.

[Sch38] O. H. Schade. Beam power tubes. http://www.clarisonus.com/Archives/TubeTheory/Schade%201938% 1938. Publication ST-59, Tube Division RCA.

[Spa48] Karl Spangenberg. *Vacuum tubes*. McGraw-Hill, 1948.

[WML95] Jr. W. Marshall Leach. Spice models for vacuum-tube amplifiers. *J. Audio Eng. Soc.*, 43:117, 1995.